



HAL
open science

Characterization of the mouse ClC-K1/Barttin chloride channel

Sébastien L'Hoste, Alexi Diakov, Olga Andrini, Mathieu Genete, Laurent Pinelli, Teddy Grand, Mathilde Keck, Marc Paulais, Laurent Beck, Christoph Korbmacher, et al.

► **To cite this version:**

Sébastien L'Hoste, Alexi Diakov, Olga Andrini, Mathieu Genete, Laurent Pinelli, et al.. Characterization of the mouse ClC-K1/Barttin chloride channel. *Biochimica et Biophysica Acta: Biomembranes*, 2013, 1828 (11), pp.2399-2409. 10.1016/j.bbamem.2013.06.012 . hal-02452579

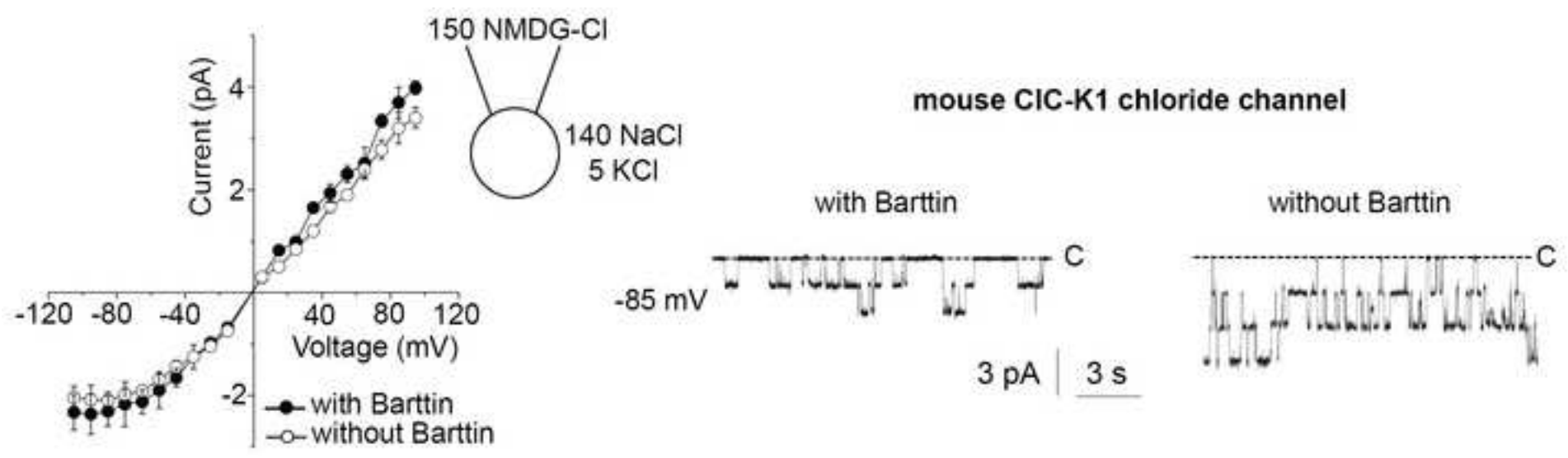
HAL Id: hal-02452579

<https://hal.sorbonne-universite.fr/hal-02452579v1>

Submitted on 24 Jan 2020

HAL is a multi-disciplinary open access archive for the deposit and dissemination of scientific research documents, whether they are published or not. The documents may come from teaching and research institutions in France or abroad, or from public or private research centers.

L'archive ouverte pluridisciplinaire **HAL**, est destinée au dépôt et à la diffusion de documents scientifiques de niveau recherche, publiés ou non, émanant des établissements d'enseignement et de recherche français ou étrangers, des laboratoires publics ou privés.



Highlights

The mouse ClC-K1 Cl⁻ channel has properties similar to those of ClC-Ka or rat ClC-K1 >
ClC-K1 has a single-channel conductance of ~40 pS and is activated on depolarization >
Insertion of the V166E mutation in ClC-K1 revealed the activity of the protopore > Barttin
increases ClC-K1 surface expression but currents are detected in its absence > The unit
conductance and voltage dependence of ClC-K1 are not affected by Barttin

Characterization of the mouse ClC-K1/Barttin chloride channel

Sébastien L'Hoste^{a,b,c}, Alexei Diakov^d, Olga Andrini^{a,b,c}, Mathieu Genete^{a,b,c}, Laurent Pinelli^{a,b,c}, Teddy Grand^{a,b,c}, Mathilde Keck^{a,b,c}, Marc Paulais^{a,b,c}, Laurent Beck^e, Christoph Korbmacher^d, Jacques Teulon^{a,b,c}, and Stéphane Lourdel^{a,b,c}.

^aUPMC Univ Paris 06, UMRS 872, Laboratoire de génomique, physiologie et physiopathologie rénales, F-75005, Paris, France.

^bINSERM, UMRS 872, Laboratoire de génomique, physiologie et physiopathologie rénales, F-75005, Paris, France.

^cCNRS, ERL 7226, Laboratoire de génomique, physiologie et physiopathologie rénales, F-75005, Paris, France.

^dInstitut für Zelluläre und Molekulare Physiologie, Waldstr 6, 91054 Erlangen, Germany.

^eUniversité de Nantes, Faculté de Chirurgie dentaire, laboratoire d'ingénierie ostéoarticulaire et dentaire, Nantes, France

Corresponding author:

Stéphane Lourdel, UMRS 872, ERL 7226, Laboratoire de génomique, physiologie et physiopathologie rénales, 15 rue de l'Ecole de Médecine, 75270 Paris cedex 06, France

Phone: 33.1.55.42.78.55

Fax: 33.1.46.33.41.72

E-mail: stephane.lourdel@upmc.fr

ABSTRACT

Several Cl⁻ channels have been described in the native renal tubule, but their correspondence with ClC-K1 and ClC-K2 channels (orthologs of human ClC-Ka and ClC-Kb), which play a major role in transcellular Cl⁻ absorption in the kidney, has yet to be established. This is partly because investigation of heterologous expression has involved rat or human ClC-K models, whereas characterization of the native renal tubule has been done in mice. Here, we investigate the electrophysiological properties of mouse ClC-K1 channels heterologously expressed in *Xenopus laevis* oocytes and in HEK293 cells with or without their accessory Barttin subunit. Current amplitudes and plasma membrane insertion of mouse ClC-K1 were enhanced by Barttin. External basic pH or elevated calcium stimulated currents followed the anion permeability sequence Cl⁻ > Br⁻ > NO₃⁻ > I⁻. Single-channel recordings revealed a unit conductance of ~40 pS. Channel activity in cell-attached patches increased with membrane depolarization (voltage for half-maximal activation: ~ -65 mV). Insertion of the V166E mutation, which introduces a glutamate in mouse ClC-K1, which is crucial for channel gating, reduced the unit conductance to ~20 pS. This mutation shifted the depolarizing voltage for half-maximal channel activation to ~ +25 mV. The unit conductance and voltage dependence of wild-type and V166E ClC-K1 were not affected by Barttin. Owing to their strikingly similar properties, we propose that the ClC-K1/Barttin complex is the molecular substrate of a chloride channel previously detected in the mouse thick ascending limb (Paulais et al., J Membr. Biol, 1990, 113:253-260).

KEYWORDS

Chloride channel, ClC, kidney, ClC-K1, patch-clamp

NON-STANDARD ABBREVIATIONS

CCD: cortical collecting duct

ClC-K: kidney chloride channel

CNT: connecting tubule

CTAL: cortical thick ascending limb

DCT: distal convoluted tubule

DIDS: 4,4'-diisothiocyanato-2,2'-stilbene disulfonic acid disodium salt

DPC: 2-(phenylamino) benzoic acid

NPPB: 5-nitro-2-(3-phenylpropylamino) benzoic acid

OMCD: outer medullary collecting duct

1. INTRODUCTION

Two Cl⁻ channels of the ClC family, ClC-K1 and ClC-K2 (or their human orthologs ClC-Ka and ClC-Kb, respectively), play a pivotal role in transcellular Cl⁻ absorption in the kidney. Located on the basolateral membrane, they are present throughout the distal nephron [1-3], but the specific distribution of each ClC-K is still uncertain owing to the lack of isoform-specific antibodies [4]. Mutations in human genes coding for ClC-Kb and the regulatory subunit, Barttin, are responsible for salt-losing tubulopathies, namely Bartter's syndrome types 3 and 4, respectively [5-7]. Rare types of Bartter's syndrome can also result from compound mutations in ClC-Kb and ClC-Ka [8]. Renal function has not been investigated in knockout mice for ClC-K2 because they die very early; ClC-K1-knockout mice display impaired urine concentration and nephrogenic diabetes insipidus [9]. In accordance with pathological and physiological data, localization studies suggest that ClC-K2 is highly expressed in the cortical part of the distal nephron, and that ClC-K1 is mostly restricted to the medullary part of the renal tubule [2, 3, 10, 11].

The functional expression of human and rat ClC-K remained controversial until their accessory subunit, Barttin, was identified. It promotes their insertion into the plasma membrane [2, 12]. This discovery made it possible to identify two fundamental properties of ClC-K channels. First, the relative permeability for anions follows the sequence Cl⁻ > Br⁻ > NO₃⁻ > I⁻ for ClC-Ka, and Cl⁻ > Br⁻ = NO₃⁻ > I⁻ for ClC-Kb; second, the currents are enhanced by a basic external pH and high external calcium concentrations [2, 12]. Interestingly, a glutamate residue that plays a critical role in the protopore gating of other ClC chloride channels is missing in ClC-K channels, where it is replaced by a valine. For this reason, it has been suggested that the two protopores in ClC-K dimers are constitutively open. Thus, the common gate (involving both subunits of the dimers) may act as the major regulator of ClC-K

channels. In recent studies on rat ClC-K1, Fahlke's group reintroduced the "gating" glutamate and observed profound effects on both conductance and gating [4, 13, 14].

We and others have identified several basolateral chloride channels in different parts of the renal tubule, particularly in the cortical thick ascending limb (CTAL), the distal convoluted tubule (DCT), the connecting tubule (CNT), and the cortical collecting duct (CCD) [15-23]. Two of these channels, with conductances of 45 pS and 9 pS, respectively, display properties that are compatible with those of ClC-K chloride channels [24].

Nevertheless, the precise molecular identity of these channels remains elusive, because heterologous expression data are incomplete and heterogeneous. Studies of recombinant channels have involved rat and human ClC-Ks, whereas most of those of the native renal tubule have involved mouse kidney. Furthermore, there are only a few single-channel recordings available for recombinant channels, and they all derive from studies on human ClC-Ka and rat ClC-K1 [4]. In this study, we investigated the properties of recombinant mouse ClC-K1 channels expressed in the presence or absence of mouse Barttin, in an attempt to establish a coherent basis for their correspondence with native chloride channels in the mouse renal tubule.

2. MATERIAL AND METHODS

2.1. Molecular biology

The mouse CIC-K1 cDNA clone (image 5042736, Invitrogen, Carlsbad, CA, USA) and mouse Barttin (a generous gift from Prof. T. J. Jentsch, MDC/FMP, Berlin, Germany) were subcloned into pSP64-S and pVITRO2 vectors, respectively, for expression in *Xenopus laevis* oocytes. Capped cRNAs were synthesized *in vitro* from wild-type and mutant CIC-K1 and Barttin vectors using the SP6 mMessage mMachine Kit (Ambion, Austin, TX, USA). To evaluate the surface expression of CIC-K1 in *Xenopus laevis* oocytes, we externally tagged CIC-K1 by introducing a FLAG epitope (DYKDDDDK) between transmembrane domains L and M (beginning at position 377). This did not interfere with their ability to generate currents.

For electrophysiological recordings, HEK293 cells were cotransfected with 1 µg of a bicistronic vector pVITRO2 containing the coding sequence of mouse CIC-K1 and mouse Barttin, and 0.3 µg of a IRES vector encoding the CD8 antigen (a generous gift from Dr. J. Barhanin, Université Nice Sophia Antipolis, Nice, France) as a transfection marker by electroporation or using X-tremeGENE9 (Roche Diagnostics, Meylan, France). Including CD8 made it possible to identify the transfected cells using anti-CD8-coated beads (Invitrogen Dynal, Oslo, Norway). Site-directed mutagenesis was performed with the Quickchange site-directed mutagenesis kit (Stratagene, La Jolla, CA, USA).

All constructs were fully sequenced.

2.2. Two-electrode voltage-clamp

Defolliculated *Xenopus laevis* oocytes were injected with 10 ng of CIC-K1 cRNA and 5 ng of Barttin cRNA. The oocytes were then kept at 17°C in modified Barth's solution

containing (in mM): 88 NaCl, 1 KCl, 0.41 CaCl₂, 0.32 Ca(NO₃)₂, 0.82 MgSO₄, 10 HEPES, pH 7.4, and supplemented with gentamycin (20 µg/ml). Three days after injection, two-electrode voltage-clamp experiments were performed using a TEV-200A amplifier (Dagan, Minneapolis, MN, USA) and PClamp 9 software (Molecular Devices, Sunnyvale, CA). Pipettes were made from borosilicate tubes (GC150T, Harvard Apparatus, Edenbridge, UK), and filled with 3 M KCl. Currents were recorded in ND96 solution containing (in mM): 96 NaCl, 2 KCl, 1.5 CaCl₂, 1 MgCl₂, 5 HEPES, pH 7.4. Currents were recorded in response to a voltage protocol consisting of 20 mV steps from -160 mV to +100 mV with a duration of 800 ms from a holding potential of -30 mV. The data were filtered at 300 Hz, and sampled using a Digidata 1320A analogue-to-digital converter (Molecular Devices, Sunnyvale, CA).

For anion replacement, 80 mM Cl⁻ was replaced by equivalent amounts of Br⁻, I⁻ or NO₃⁻. HEPES was replaced by equimolar MES for solutions at pH 5.4-6.4, or by Tris for solutions at pH 8.4. Where appropriate, calcium acetate was added to the ND96 solution to increase the extracellular calcium concentration. The permeability ratios of various anions (X⁻) relative to that of Cl⁻ (P_{X^-}/P_{Cl^-}) were calculated using the modified Goldman-Hodgkin-Katz equation [25]:

$$\frac{P_{X^-}}{P_{Cl^-}} = \frac{(104 \times e^{40 \times (E_1 - E_2) - 24})}{80}$$

Where E_1 and E_2 are the reversal potentials for Cl⁻ and X⁻, respectively.

Chloride channel inhibitors were purchased from Sigma-Aldrich (Saint-Quentin Fallavier, France). DPC, at a concentration of 0.5 M, and NPPB, at a concentration of 0.1 M, were dissolved in DMSO. DMSO (at the maximum concentration of 0.2% used for 10⁻³ M DPC) had no effect on channel activity.

2.3. Whole-cell recording

HEK293 cells were transiently transfected by electroporation, and plated on 35-mm plastic Petri culture dishes. 20 h after transfection, the Petri dishes were mounted on the inverted stage of a microscope. The bath solution contained (in mM): 140 NaCl, 2 CaCl₂, 1 MgCl₂, 22 Sucrose, 10 HEPES, pH 7.4. HEPES was replaced by TRIS for solutions at pH 9.0. For the chloride substitution experiments, 140 NaCl was replaced by 140 NaI. The pipette solution contained (in mM): 150 NMDG-Cl, 1 MgCl₂, 2 EGTA, 1 Mg-ATP, 10 HEPES, pH 7.4 or 33 CsCl, 100 NaGluconate, 1 MgCl₂, 2 EGTA, 1 Mg-ATP, and 10 HEPES, pH 7.0. Standard whole-cell recordings were performed using an Axopatch 200B (Molecular Devices, Sunnyvale, CA) and PClamp 9 software (Molecular Devices, Sunnyvale, CA). The bath was earthed *via* an agar 3 M agar bridge. Patch-clamp pipettes had resistances of 2-3 MΩ. The following pulse protocol was used: from a holding potential of -30 mV, after a pre-pulse to +65 mV for 30 ms, voltage was stepped from -115 mV to +105 mV in 20 mV increments for 160 ms, and followed by a pulse to +105 mV.

2.4. Single-channel recordings in outside-out patches of *Xenopus laevis* oocytes

Recordings in outside-out membrane patches of mClC-K1 and mBarttin expressing oocytes were performed essentially as described previously using a conventional patch-clamp technique [26, 27]. Patch pipettes were pulled from borosilicate glass capillaries, and had a tip diameter of about 1-1.5 μm after fire polishing. Pipettes were filled with the KCl pipette solution (in mM: 55 KCl, 35 K-gluconate, 5 NaCl, 1.2 MgCl₂, 2 EGTA, 10 HEPES, pH 7.28). Seals were routinely formed in a low sodium NMDG-Cl bath solution (in mM: 95 NMDG-Cl, 1 NaCl, 4 KCl, 1 MgCl₂, 1 CaCl₂, 10 HEPES, pH 7.4). In the NaCl bath solution, 95 mM NMDG-Cl was replaced by 95 mM NaCl. In the NaBr, NaI and NaNO₃ bath solutions, 95 mM NMDG-Cl was replaced by 10 mM NaCl and by 85 mM NaBr, 85 mM NaI and

85 mM NaNO₃, respectively. After seal formation, the bath solution was changed to the NaCl, NaI, NaBr or NaNO₃ bath solutions. Single-channel current data were initially filtered at 3 kHz and sampled at 9 kHz. Current traces were re-filtered at 250 Hz to resolve the single channel current amplitude (*i*).

2.5. Single-channel recordings in HEK293 cells

HEK293 cells were transiently transfected using X-tremeGENE9 according to the Manufacturer's instructions (Roche Diagnostics, Meylan, France). Recordings were performed two days after transfection. The cells were initially bathed in physiological saline containing (in mM): 140 NaCl, 5 KCl, 1 CaCl₂, 1 MgCl₂, 10 glucose, 10 HEPES, pH 7.4.

The pipettes made from borosilicate tubes (GC150T, Harvard Apparatus, Edenbridge, Kent) were coated with Sylgard (Dow Corning, Seneffe, Belgium), and polished just before use. The pipettes were filled with a high-Cl⁻ solution containing (in mM): 150 NMDG-Cl, 1 MgCl₂, 10 glucose, and 10 HEPES, pH 7.4. The solutions used to characterize channel properties in the inside-out configuration contained 2 mM EGTA and no calcium. To record the currents, we used a RK 400 patch-clamp amplifier (Bio-logic, Claix, France) and PClamp 9 software (Molecular Devices, Sunnyvale, CA). Currents were filtered at 300 or 500 Hz, and were sampled at 1-2 kHz using a Digidata 1322A analogue-to-digital converter (Molecular Devices, Sunnyvale, CA). The mean current (*I*) passing through *N* channels was used to calculate the normalized current (*NPo*) according to the equation $NPo = I/i$, where *i* is the unitary current amplitude. The relationship between *NPo* and voltage (*V*) was fitted using a Boltzmann equation:

$$NPo(V) = NPo_{\min} + \frac{NPo_{\max} - NPo_{\min}}{1 + \exp((V_{1/2} - V)/k)}$$

where V is the membrane voltage, $NP_{O_{min}}$ and $NP_{O_{max}}$ are the minimum and maximum values of NP_O , respectively, $V_{1/2}$ is the half-maximal activation voltage, and k is the slope factor of the voltage dependence. The liquid junction potentials were calculated with PClamp 9 and corrected accordingly.

2.6. Measurement of surface expression

Experiments were performed as previously described [28], using an anti-FLAG M2 monoclonal antibody (Sigma-Aldrich, St. Louis, MO, USA) as the primary antibody, and a peroxidase-conjugated goat anti-mouse antibody (Santa Cruz Biotechnology Inc., Santa Cruz, CA, USA) as the secondary antibody. Chemiluminescence was quantified in a Turner TD-20/20 luminometer (Turner Designs, Sunnyvale, CA, USA) by placing individual oocytes in 50 μ l of SuperSignal Elisa Femto Maximum Sensitivity Substrate Solution (Pierce, Rockford, IL, USA).

2.7. Statistics

Results are shown as mean \pm SEM. n indicates the number of experiments. Statistical significance was determined by a paired Student's t -test using SigmaStat software (SPSS, Erkrath, Germany). A value of $P < 0.05$ was considered to be significant.

3. RESULTS

3.1. Functional characterization of mClC-K1 channels at the whole-cell level in *X. laevis* oocytes

We expressed mouse ClC-K1 channels (mClC-K1) in *X. laevis* oocytes, with or without mouse Barttin (mBarttin), to characterize their conductive properties at the whole cell level. As previously reported for rat ClC-K1 (rClC-K1) [12, 25, 29], mClC-K1 alone induced small but significant currents, while co-expression with mBarttin markedly increased the current intensity ($n = 30$; Fig. 1A, B). In human Barttin, mutation of a putative proline-tyrosine (PY) motif (Y98A) further enhances hClC-K currents [2]. Likewise, mClC-K1 currents were also greater in oocytes expressing mBarttin mutated at the equivalent position (Y95A) than in oocytes expressing non-mutated Barttin ($n = 30$; Fig. 1A, B). mBarttin and Y95A mBarttin alone produced currents that were not different from those in non-injected oocytes ($n = 30$; Fig. 1A, B). There was a time-dependent increase in the mClC-K1 current at the highest positive voltages, and the corresponding current/voltage relationships showed outward rectification (Fig. 1B), which was reminiscent of hClC-Kb, rather than of hClC-Ka or rClC-K1, which display linear or slightly inwardly rectifying currents [2, 12].

Using a chemiluminescence assay and taking advantage of the extracellular FLAG-tag placed on mClC-K1, we observed that mBarttin and Y95A mBarttin increased plasma membrane expression of ClC-K1 by ~177% ($n = 30$) and ~393% ($n = 30$), respectively (Fig. 2). Since surface expression correlated with channel currents (Fig. 2), the significant increase in current amplitudes of mClC-K1 channels could be ascribed to increased surface expression by mBarttin.

We then investigated the key electrophysiological properties of mClC-K1 in oocytes injected with the Y95A mBarttin mutant. We first assessed the selectivity among anions from

current-voltage measurements when most of the Cl^- in the bathing solution (80 mM) had been replaced by the test anion (Fig. 3A). The analysis of the data yielded $P_{\text{I}^-}/P_{\text{Cl}^-} = 0.20 \pm 0.05$ ($n = 35$), $P_{\text{NO}_3^-}/P_{\text{Cl}^-} = 0.35 \pm 0.18$ ($n = 11$), and $P_{\text{Br}^-}/P_{\text{Cl}^-} = 0.86 \pm 0.14$ ($n = 15$). This indicates a permeability sequence of $\text{Cl}^- > \text{Br}^- > \text{NO}_3^- > \text{I}^-$, which is similar to that observed previously for rClC-K1, for hClC-Ka [2, 12, 25], and for the Cl^- channel in the basolateral membrane of mouse CTAL [19].

Also consistently with previous results [2, 12, 25, 30], we found that the currents elicited by mClC-K1/Y95A mBarttin channels decreased by $65 \pm 1\%$ ($n = 6$) in response to extracellular acidification (pH 6.0), and by $50 \pm 1\%$ ($n = 6$) in response to the removal of extracellular calcium (Fig. 3B). They increased by $55 \pm 9\%$ ($n = 9$) at pH 8.0 and by $76 \pm 6\%$ ($n = 6$) in the presence of 5 mM of extracellular calcium (Fig. 3B). Similar results were obtained in the absence of mBarttin (Fig. 3B) ($n = 11$).

We investigated the effects of several classical Cl^- channel blockers by adding them to the extracellular solution. At +60 mV, DIDS (100 μM) reduced mClC-K1/Y95A mBarttin currents by $53 \pm 1\%$ ($n = 6$) (not shown). Both DPC (1 mM) and NPPB (100 μM) blocked the channels to a lesser extent, reducing currents by $34 \pm 1\%$ ($n = 6$) and $42 \pm 1\%$ ($n = 6$), respectively (not shown). Qualitatively similar results have been obtained on rClC-K1 [25, 29, 31], except for DPC, the effect of which is particularly tenuous as far as mClC-K1 is concerned.

Taking these results as a whole, mClC-K1 displays the major hallmarks of recombinant ClC-K1 channels, including $\text{Cl}^- > \text{Br}^- > \text{NO}_3^- > \text{I}^-$ anion selectivity, sensitivity to external pH and calcium, and increased expression at the membrane with Barttin. In addition, the anion selectivity sequence is identical to that found by Paulais et al. [19] for the 45-pS native Cl^- channel, and slightly different from that found for the 9-pS channel [21, 22, 23].

3.2. Single-channel recordings of mCIC-K1 channels in *X. laevis* oocytes

To investigate the single-channel properties of mCIC-K1/mBarttin heterologously expressed in *Xenopus laevis* oocytes, we performed outside-out patch clamp experiments essentially as previously described [26, 27]. Fig. 4A shows a representative single-channel current trace recorded at a holding potential of -70 mV. The corresponding binned current amplitude histogram is shown below the current trace. These data indicate that single-channel events with two different current amplitudes can be detected, as expected, for a double-barrelled channel of the CIC ion channel family [32-34]. In similar recordings, single-channel current amplitude of events with “full” and “half” openings averaged -1.9 ± 0.08 pA ($n = 11$) and -0.98 ± 0.04 pA ($n = 11$), respectively.

Fig. 4B shows representative, single-channel, current traces recorded at different holding potentials in an outside-out patch from another oocyte also expressing mCIC-K1/mBarttin channels. Fig. 4C shows averaged current/voltage relationships ($n = 5-11$) obtained from similar recordings as shown in Fig. 4B. These data demonstrate that mCIC-K1/mBarttin channels has single-channel “full” and “half” conductances of 44.9 ± 1.4 pS ($n = 12$) and 23.9 ± 0.9 pS ($n = 12$), respectively. The anion selectivity of mCIC-K1 expressed in oocytes, when assessed at the single-channel level, was compatible with that measured using voltage-clamp whole-cell recordings. This is illustrated by the representative single-channel current traces shown in Fig. 5 (holding potential: $+50$ mV). At this potential, with Γ in the bath solution, no single-channel event was detected (Fig. 5A). With Br^- in the bath, the “full” and “half” single-channel current amplitudes (i_{Br^-} : 1.3 and 0.65 pA, respectively) were ~46% lower than the same currents in the presence of Cl^- (i_{Cl^-} : 2.3 and 1.25 pA, respectively) (Fig. 5B). Similar observations were made in a total of 5 experiments.

The unit conductance of mCIC-K1, as assessed in the oocyte expression system, is compatible with that of the native 45-pS Cl^- channel [19].

3.3. Whole-cell recordings of mClC-K1 channels in HEK293 cells

Whole-cell current recordings were conducted in HEK293 cells, and revealed linear currents when the pipette was filled with 150 mM Cl⁻ ($n = 4$) (Fig. 6A, B). The whole-cell currents were in the same range as the rat ClC-K1 currents recorded previously by Scholl *et al.* [13]. They were significantly increased by elevating the extracellular pH to 9.0 ($n = 4$), and were significantly reduced by the partial replacement of extracellular Cl⁻ by I⁻ ($n = 4$) [2, 12, 25, 30]. In contrast to what is observed in the oocyte expression system, no time-dependent relaxation components were visible on the current traces (Fig. 6A). That the shape of the currents depended on the expression system had also been noted previously for ClC-Ka and ClC-Kb [4]. ClC-Ka also exhibits a linear current-voltage relationship with 150 mM Cl⁻ in the pipette, while rClC-K1 is inwardly rectifying [13, 14]. This difference might be attributable to the fact that rClC-K1, which is clearly voltage-dependent when transfected in cultured cells, is activated in response to hyperpolarization [13, 14, 35]. For mClC-K1, the current/voltage relationships (Fig. 6C) showed outward rectification in the presence of a low internal Cl⁻ solution (35 mM) ($n = 7$).

These results suggest that HEK293 cells is a suitable model for studying mClC-K1 currents at the single-channel level.

3.4. Conductive properties of mClC-K1 channels at the single-channel level in HEK293 cells

Fig. 7A shows typical recordings of mClC-K1/mBarttin channel activity on cell-attached membrane patches from HEK293-transfected cells bathed with physiological saline solution, with the pipette filled with a high-Cl⁻ solution. Under these conditions, we observed highly active channels (Fig. 7A). It is apparent that most mClC-K1 channels displayed “full” opening when expressed in HEK293 cells. The current/voltage relationship displayed rather marked outward rectification, probably due to low [Cl⁻]_i (Fig. 7B). The unit conductance of

the “full” openings, measured in the linear part of the current-voltage relationship, averaged 41.9 ± 1.5 pS ($n = 11$). The reversal potential (-1.8 ± 1.2 mV, $n = 11$) was close to zero. Fig. 7B also shows the linear current/voltage relationship obtained in the inside-out configuration when high-Cl⁻ solutions were present on both sides of the membrane patch. The unit conductance (44.4 ± 1.4 pS, $n = 7$) was not statistically different from that determined in the cell-attached configuration.

Channel activity increased at positive potentials (Fig. 7A). This was typically observed in 7 cell-attached patches, in which we investigated the voltage dependence of the *NPo*. The mean relationship between *NPo* and voltage is given in Fig. 7C. Fitting our data with a Boltzmann equation yielded a half-maximal activation voltage ($V_{1/2}$) of -65.6 mV. Voltage dependence was no longer observed in the inside-out configuration, suggesting that it is mediated by some intracellular factor (Fig. 7C).

To investigate the possible modulation of mClC-K1 channel gating and unit conductance by mBarttin [13, 14], we performed single-channel analysis in cell-attached membrane patches using HEK293-transfected cells expressing mClC-K1 alone. Fig. 7B and Fig 7C show that neither the unit conductance (38.1 ± 1.4 pS; $n = 4$) nor the voltage dependent activation of the channel ($V_{1/2} = -70.1$ mV) were significantly modified compared to mClC-K1 co-expressed with Barttin.

These results, as a whole, show that the single-channel properties of mClC-K1/mBarttin are strikingly similar to those of the 45-pS native Cl⁻ channel [19]. In particular, the open probability has values close to those measured in the mouse CTAL [19] when measured on HEK293 cells.

3.5. Conductive properties of V166E mCIC-K1 mutant channels in HEK293 cells

We anticipated that introducing a glutamate at a position equivalent to 166 might create a protopore gate, making it easier to detect the openings of the protopores. In CIC-0, changes in the amino acid at the equivalent position 166 did not alter the protopore conductance [34]. In a first step, we performed whole-cell recordings in HEK293 cells using 150 mM Cl⁻ in the pipette solution (Fig. 8). The V166E mutant displayed clear outward rectification under these conditions suggesting that the gating of the channel has been modified in agreement with our hypothesis.

Fig. 9A shows representative cell-attached current recordings from HEK-293 cells transfected with V166E mCIC-K1/mBarttin channels. The mean current-voltage relationship was essentially linear (Fig. 8B) and reversed at -1.4 ± 2.1 mV; a unit conductance of 19.9 ± 1.3 pS was computed ($n = 4$). Channel activity increased at positive voltages ($n = 4$) (Fig. 8C). The best fit of our data indicated that the half-maximal activation voltage of the mutant channel was shifted to more positive potentials as compared to WT mCIC-K1/mBarttin ($V_{1/2} = 24.9$ mV). Voltage dependence persisted in the cell-free mode (not shown). In contrast, two other point mutations introduced at position 166 did not have the same effect as V166E. The V166L mutation did not significantly modify the unit conductance (38.5 ± 4.0 pS, $n = 3$; not shown), and the V166M only moderately modified the unit conductance (38.5 and 29.5 pS, $n = 2$; not shown). We can therefore reasonably conclude that the V166E mutation revealed the activity of the channel protopore by introducing *de novo* protopore gating.

We also recorded single-channel activity from cell-attached patches from HEK-293 cells transfected with V166E mCIC-K1 without mBarttin: there was no significant change in unit conductance (18.3 ± 0.7 pS; $n = 4$) (Fig. 9B), channel voltage dependence ($n = 4$) (Fig. 9C), or for half-maximal voltage activation ($V_{1/2} = 21.7$ mV).

4. DISCUSSION

4.1. The apparent properties of mClC-K1 partly depend on the heterologous expression model

Fahlke & Fischer [4] have previously pointed out that there are clear kinetic and current/voltage relationships differences between ClC-K channels expressed in *X. laevis* oocytes and those expressed in mammalian cells. This was also observed for the mouse ClC-K1, but can be partly explained by the differing experimental conditions.

In HEK293 cells, mClC-K1/mBarttin yields linear currents with 150 mM Cl⁻ in the pipette and outwardly rectifying currents in the presence of low Cl⁻ (35 mM), a situation closer to that seen in the oocytes. Indeed, in *X. laevis* oocytes where the intracellular Cl⁻ is around 30-50 mM, currents are outwardly rectifying. Furthermore, single-channel current amplitudes in the cell attached mode also showed outward rectification (low intracellular Cl⁻ concentration). We can therefore assume that the discrepancy in the shapes of the current/voltage relationships obtained for whole-cell currents between heterologous expression models is due to normal, Goldman-type rectification, and is related to the level of intracellular chloride.

The time-dependent components that increase mClC-K1 currents at positive voltages in *X. laevis* oocytes suggest activation at depolarizing voltages, which was not observed in whole-cell recordings from HEK293 cells. However, the NP_o of the mClC-K1 increased in response to depolarization in cell-attached patches from HEK293 cells, a condition in which the cell is intact (as for oocyte recordings). We may speculate that cell dialysis during whole-cell recording removed some component necessary for voltage gating. Indeed, the voltage-dependence that was observed in cell-attached patches also disappeared in inside-out patches.

In contrast to cell-attached recordings of HEK 293 cells, recordings from outside-out patches from oocytes always displayed very low open probability. A very low open

probability has also been observed when recording ClC-Ka from cell-free patches obtained on oocytes [36]. In contrast, ClC-Ka single-channel activity recorded from patches attached to mammalian cultured cells is high (see for instance, [14]). It may be speculated that, for some unknown reason, the mClC-K1 channels experience rundown following excision. Overall, mClC-K1/Barttin expressed in HEK293 cells more faithfully reflects the native 45-pS Cl⁻ channel.

4.2. The properties of mouse ClC-K1 are comparable to those of recombinant human ClC-Ka and rat ClC-K1

So far, only the electrophysiological properties of human and rat ClC-K channels have been investigated. Previous studies have demonstrated that recombinant hClC-Ka and rClC-K1 have identical properties at the whole-cell level in terms of anion selectivity, sensitivity to external pH and Ca²⁺, and sensitivity to chloride channels blockers as DIDS and NPPB [2, 12, 25, 30, 31, 37]. However, rClC-K1 channels are active in the absence of Barttin; whereas hClC-Ka channels need Barttin to become anion conductive at the cell surface [2, 12, 30]. Our findings provide evidence that mClC-K1 shares many of the properties of hClC-Ka and rClC-K1 at the whole cell level, including the anion selectivity sequence (Cl⁻ > Br⁻ > NO₃⁻ > I⁻), being activated at external basic pH or elevated Ca²⁺, and sensitivity to DIDS and NPPB. We also observed that mClC-K1, like rClC-K1, is active without mBarttin. There are also small differences that concern the voltage dependence (activation by depolarization for mClC-K1, by hyperpolarization for rat ClC-K1) and unitary conductances (40 pS for mClC-K1, 33 pS for rClC-K1 and 26 pS for hClC-Ka) [13, 14].

4.3. Single-channel activity in HEK293 cells reflects dimer gating of mClC-K1

ClC channels, which function as dimer complexes, are endowed with two voltage-dependent gates, the protopore (“fast”) gate, and the common (“slow”) gate [38]. Protopore gating requires the presence of a glutamate at equivalent position 166. Indeed, substituting glutamate for valine (or alanine) in ClC-0 abolishes most of the protopore gating, and only brief closures of the protopores are detected [34]. Since the ClC-K channels have a valine residue at position 166 rather than a glutamate, it may be anticipated that their voltage dependence is due to common gating. Accordingly, the experiments we performed in the cell-attached mode in HEK293 transfected cells showed that half openings and closings of mClC-K1 due to protopore gating were rarely detected in these recordings. As a consequence, the NP_o values found in these experiments essentially reflect the activity of the common gate.

Thus, the common gate of mClC-K1 channels is moderately activated by depolarization. It is noteworthy that the half-maximal activation voltage $V_{1/2}$ (~ -65 mV), which is close to the resting membrane potential in renal cells, suggests that this regulation might be physiologically relevant. In sharp contrast, rClC-K1 channels are activated by hyperpolarization [13, 14]. In this case, the voltage dependence is due to the fast gate, the slow gate being voltage-independent [14]. This may indicate that ClC-K regulation differs in different species. It could also indicate that the protopore gate, which according to Fahlke et al. [13, 14] is activated by hyperpolarization, might contribute to the total open probability, notably under physiological circumstances that were not encountered in our experiments.

4.4. Barttin has no influence on ClC-K1 channel gating or conductance

Barttin is an accessory regulatory subunit that is essential for the functional expression of hClC-Ka and hClC-Kb, and which also increases the current generated by rClC-K1 [14]. We also observed that mClC-K1 currents were greater in the presence of Barttin. However,

mClC-K1, like rClC-K1, carried currents in the absence of Barttin when expressed in heterologous expression systems. Furthermore, we observed that mClC-K1 currents were still stimulated by external calcium and inhibited by protons in the absence of Barttin. Consequently, this must be an intrinsic property of the ClC-K, as has been reported elsewhere [12].

Barttin also modulates ClC-K gating [14]. Fahlke et al. initially reported that rClC-K1 was activated by hyperpolarization in both the presence and the absence of Barttin [13]. Later on, however, they reported that the voltage dependence of rClC-K1 expressed alone was not voltage dependent [14]. In the absence of Barttin, V166E rClC-K1 channels were activated by membrane hyperpolarization, whereas in the presence of Barttin, mutant ClC-K1 channels were activated by membrane depolarization [13, 14]. In the present study, the voltage dependence of wild-type and V166E mClC-K1 channels was not modified in the absence of Barttin.

Thus, the main effect of Barttin is to increase the number of mClC-K1 channels in the plasma membrane. However, the fact that mClC-K1, like rClC-K1, is active in the absence of Barttin raises questions about the physiological role of this accessory subunit. The observation that Barttin-knockout mice suffer from severe renal salt and water loss, and die within a few days after birth demonstrates that Barttin is strictly necessary for ClC-K function in mouse kidneys [39]. There are two possible explanations. First, in the absence of Barttin, the expression of ClC-K1 at the plasma membrane is insufficient to sustain sufficient chloride transport. A possible alternative explanation, although the two are not mutually exclusive, could be that Barttin is required for ClC-K1 to be addressed specifically to the basolateral membrane. Indeed, some mutations of *BSND* result in the increased expression of ClC-Kb at the apical membrane [35].

4.5. *mClC-K1* underlies the native 45-pS chloride channel

Several chloride channels have been identified in the basolateral membranes of microdissected mouse renal tubules by means of single-channel recordings.

The first Cl^- channel we reported in mouse CTAL had a unit conductance of 45 pS, and a permeability sequence $\text{Cl}^- > \text{Br}^- > \text{NO}_3^-$ [19]. No current was recorded in the presence of I^- , suggesting that this anion has a blocking effect. Importantly, this channel was activated by depolarization, a property that disappeared after excision of the membrane patch.

A second Cl^- channel has been detected throughout the length of the distal nephron [21-23]. It has a conductance of 9 pS. We have previously suggested that it is underpinned by *ClC-K2* on the basis of its anion selectivity sequence and the fact that it is distributed throughout the renal tubule [24]. This remains to be directly proved, since recombinant *ClC-K2* has not so far been studied at the single-channel level. Finally, we should mention that a third Cl^- channel has been reported, the properties of which are incompatible with those of the *ClC-Ks* [20, 24]

4.6. *Physiological roles of ClC-K1*

Initially, *ClC-K1* expression was thought to be restricted to the thin ascending limb [30], where it provides a transcellular route for Cl^- absorption, while Na^+ follows *via* the paracellular pathway [40]. Due to this strategic localization, *ClC-K1* was believed to play a major role in urine concentration [9, 40].

The current view, however, proposes that *ClC-K1* is more widely distributed along the renal tubule than previously thought [2, 3, 12]. In particular, it is also present in the MTAL and CTAL, where we have detected its single-channel properties [19]. This segment absorbs 25% of filtered NaCl by the operation of a $\text{Na}^+ - \text{K}^+ - 2\text{Cl}^-$ cotransporter at the apical membrane, and the presence of $\text{Na}^+ - \text{K}^+$ ATPase at the basolateral membrane. Cl^- conductance is

necessary for the basolateral step of Cl^- absorption. ClC-K1 probably plays only a minor role, since Akzaki et al. [41] showed that there was no sodium loss in $\text{ClC-K1}^{-/-}$ mice. Accordingly, two additional Cl^- channels are thought to be expressed in the CTAL [24], which may compensate for the absence of ClC-K1 .

ACKNOWLEDGMENTS

This work was supported by grants from the Agence Nationale de la Recherche (ANR) (ANR07-PHYSIO-008-2 and BLAN 2010-111201), and by a grant from the BHFZ (Bayerisch-Französisches Hochschulzentrum; FK-13/09). S. L'Hoste and O. Andrini hold ANR postdoctoral fellowships, and M. Keck, T. Grand and L. Pinelli PhD fellowships from the Ministère de l'Enseignement Supérieur et de la Recherche. The English text was edited by M. Ghosh.

REFERENCES

- [1] A. Vandewalle, F. Cluzeaud, M. Bens, S. Kieferle, K. Steinmeyer, T.J. Jentsch, Localization and induction by dehydration of ClC-K chloride channels in the rat kidney, *Am J Physiol* 272 (1997) F678-688.
- [2] R. Estevez, T. Boettger, V. Stein, R. Birkenhager, E. Otto, F. Hildebrandt, T.J. Jentsch, Barttin is a Cl⁻ channel beta-subunit crucial for renal Cl⁻ reabsorption and inner ear K⁺ secretion, *Nature* 414 (2001) 558-561.
- [3] K. Kobayashi, S. Uchida, S. Mizutani, S. Sasaki, F. Marumo, Intrarenal and cellular localization of CLC-K2 protein in the mouse kidney, *J Am Soc Nephrol* 12 (2001) 1327-1334.
- [4] C. Fahlke, M. Fischer, Physiology and pathophysiology of ClC-K/barttin channels, *Front Physiol* 1 (2010) 155.
- [5] D.B. Simon, R.S. Bindra, T.A. Mansfield, C. Nelson-Williams, E. Mendonca, R. Stone, S. Schurman, A. Nayir, H. Alpay, A. Bakaloglu, J. Rodriguez-Soriano, J.M. Morales, S.A. Sanjad, C.M. Taylor, D. Pilz, A. Brem, H. Trachtman, W. Griswold, G.A. Richard, E. John, R.P. Lifton, Mutations in the chloride channel gene, CLCNKB, cause Bartter's syndrome type III, *Nat Genet* 17 (1997) 171-178.
- [6] M. Konrad, M. Vollmer, H.H. Lemmink, L.P. van den Heuvel, N. Jeck, R. Vargas-Poussou, A. Lakings, R. Ruf, G. Deschenes, C. Antignac, L. Guay-Woodford, N.V. Knoers, H.W. Seyberth, D. Feldmann, F. Hildebrandt, Mutations in the chloride channel gene CLCNKB as a cause of classic Bartter syndrome, *J Am Soc Nephrol* 11 (2000) 1449-1459.
- [7] R. Birkenhager, E. Otto, M.J. Schurmann, M. Vollmer, E.M. Ruf, I. Maier-Lutz, F. Beekmann, A. Fekete, H. Omran, D. Feldmann, D.V. Milford, N. Jeck, M. Konrad, D. Landau, N.V. Knoers, C. Antignac, R. Sudbrak, A. Kispert, F. Hildebrandt, Mutation of BSND causes Bartter syndrome with sensorineural deafness and kidney failure, *Nat Genet* 29 (2001) 310-314.
- [8] K.P. Schlingmann, M. Konrad, N. Jeck, P. Waldegger, S.C. Reinalter, M. Holder, H.W. Seyberth, S. Waldegger, Salt wasting and deafness resulting from mutations in two chloride channels, *N Engl J Med* 350 (2004) 1314-1319.
- [9] Y. Matsumura, S. Uchida, Y. Kondo, H. Miyazaki, S.B. Ko, A. Hayama, T. Morimoto, W. Liu, M. Arisawa, S. Sasaki, F. Marumo, Overt nephrogenic diabetes insipidus in mice lacking the CLC-K1 chloride channel, *Nat Genet* 21 (1999) 95-98.
- [10] S. Adachi, S. Uchida, H. Ito, M. Hata, M. Hiroe, F. Marumo, S. Sasaki, Two isoforms of a chloride channel predominantly expressed in thick ascending limb of Henle's loop and collecting ducts of rat kidney, *J Biol Chem* 269 (1994) 17677-17683.
- [11] S. Kieferle, P. Fong, M. Bens, A. Vandewalle, T.J. Jentsch, Two highly homologous members of the ClC chloride channel family in both rat and human kidney, *Proc Natl Acad Sci U S A* 91 (1994) 6943-6947.
- [12] S. Waldegger, N. Jeck, P. Barth, M. Peters, H. Vitzthum, K. Wolf, A. Kurtz, M. Konrad, H.W. Seyberth, Barttin increases surface expression and changes current properties of ClC-K channels, *Pflugers Arch* 444 (2002) 411-418.
- [13] U. Scholl, S. Hebeisen, A.G. Janssen, G. Muller-Newen, A. Alekov, C. Fahlke, Barttin modulates trafficking and function of ClC-K channels, *Proc Natl Acad Sci U S A* 103 (2006) 11411-11416.
- [14] M. Fischer, A.G. Janssen, C. Fahlke, Barttin activates ClC-K channel function by modulating gating, *J Am Soc Nephrol* 21 (2010) 1281-1289.

- [15] C.J. Winters, W.B. Reeves, T.E. Andreoli, Cl⁻ channels in basolateral renal medullary membranes: III. Determinants of single-channel activity, *J Membr Biol* 118 (1990) 269-278.
- [16] C.J. Winters, W.B. Reeves, T.E. Andreoli, Cl⁻ channels in basolateral renal medullary membrane vesicles: IV. Analogous channel activation by Cl⁻ or cAMP-dependent protein kinase, *J Membr Biol* 122 (1991) 89-95.
- [17] C.J. Winters, W.B. Reeves, T.E. Andreoli, Cl⁻ channels in basolateral TAL membranes. XIV. Kinetic properties of a basolateral MTAL Cl⁻ channel, *Kidney Int* 55 (1999) 1444-1449.
- [18] R. Sauve, S. Cai, L. Garneau, H. Klein, L. Parent, pH and external Ca²⁺ regulation of a small conductance Cl⁻ channel in kidney distal tubule, *Biochim Biophys Acta* 1509 (2000) 73-85.
- [19] M. Paulais, J. Teulon, cAMP-activated chloride channel in the basolateral membrane of the thick ascending limb of the mouse kidney, *J Membr Biol* 113 (1990) 253-260.
- [20] R. Guinamard, A. Chraïbi, J. Teulon, A small-conductance Cl⁻ channel in the mouse thick ascending limb that is activated by ATP and protein kinase A, *J Physiol* 485 (1995) 97-112.
- [21] S. Lourdel, M. Paulais, P. Marvao, A. Nissant, J. Teulon, A chloride channel at the basolateral membrane of the distal-convoluted tubule: a candidate ClC-K channel, *J Gen Physiol* 121 (2003) 287-300.
- [22] A. Nissant, S. Lourdel, S. Baillet, M. Paulais, P. Marvao, J. Teulon, M. Imbert-Teboul, Heterogeneous distribution of chloride channels along the distal convoluted tubule probed by single-cell RT-PCR and patch clamp, *Am J Physiol Renal Physiol* 287 (2004) F1233-1243.
- [23] A. Nissant, M. Paulais, S. Lachheb, S. Lourdel, J. Teulon, Similar chloride channels in the connecting tubule and cortical collecting duct of the mouse kidney, *Am J Physiol Renal Physiol* 290 (2006) F1421-1429.
- [24] J. Teulon, S. Lourdel, A. Nissant, M. Paulais, R. Guinamard, P. Marvao, M. Imbert-Teboul, Exploration of the basolateral chloride channels in the renal tubule using the patch-clamp technique, *Nephron Physiol* 99 (2005) p64-68.
- [25] S. Waldegger, T.J. Jentsch, Functional and structural analysis of ClC-K chloride channels involved in renal disease, *J Biol Chem* 275 (2000) 24527-24533.
- [26] A. Diakov, K. Bera, M. Mokrushina, B. Krueger, C. Korbmacher, Cleavage in the {gamma}-subunit of the epithelial sodium channel (ENaC) plays an important role in the proteolytic activation of near-silent channels, *J Physiol* 586 (2008) 4587-4608.
- [27] B. Krueger, S. Haerteis, L. Yang, A. Hartner, R. Rauh, C. Korbmacher, A. Diakov, Cholesterol depletion of the plasma membrane prevents activation of the epithelial sodium channel (ENaC) by SGK1, *Cell Physiol Biochem* 24 (2009) 605-618.
- [28] N. Zerangue, B. Schwappach, Y.N. Jan, L.Y. Jan, A new ER trafficking signal regulates the subunit stoichiometry of plasma membrane K(ATP) channels, *Neuron* 22 (1999) 537-548.
- [29] S. Uchida, S. Sasaki, T. Furukawa, M. Hiraoka, T. Imai, Y. Hirata, F. Marumo, Molecular cloning of a chloride channel that is regulated by dehydration and expressed predominantly in kidney medulla, *J Biol Chem* 269 (1994) 19192.
- [30] S. Uchida, S. Sasaki, K. Nitta, K. Uchida, S. Horita, H. Nihei, F. Marumo, Localization and functional characterization of rat kidney-specific chloride channel, ClC-K1, *J Clin Invest* 95 (1995) 104-113.
- [31] A. Liantonio, M. Pusch, A. Picollo, P. Guida, A. De Luca, S. Pierno, G. Fracchiolla, F. Loiodice, P. Tortorella, D. Conte Camerino, Investigations of pharmacologic properties of the renal ClC-K1 chloride channel co-expressed with barttin by the use

- of 2-(p-Chlorophenoxy)propionic acid derivatives and other structurally unrelated chloride channels blockers, *J Am Soc Nephrol* 15 (2004) 13-20.
- [32] L. Feng, E.B. Campbell, Y. Hsiung, R. MacKinnon, Structure of a eukaryotic CLC transporter defines an intermediate state in the transport cycle, *Science* 330 (2010) 635-641.
- [33] C. Miller, Open-state substructure of single chloride channels from Torpedo electroplax, *Philos Trans R Soc Lond B Biol Sci* 299 (1982) 401-411.
- [34] R. Dutzler, E.B. Campbell, R. MacKinnon, Gating the selectivity filter in ClC chloride channels, *Science* 300 (2003) 108-112.
- [35] A.G. Janssen, U. Scholl, C. Domezeyer, D. Nothmann, A. Leinenweber, C. Fahlke, Disease-causing dysfunctions of barttin in Bartter syndrome type IV, *J Am Soc Nephrol* 20 (2009) 145-153.
- [36] G. Zifarelli, A. Liantonio, A. Gradogna, A. Picollo, G. Gramegna, M. De Bellis, A.R. Murgia, E. Babini, D.C. Camerino, M. Pusch, Identification of sites responsible for the potentiating effect of niflumic acid on ClC-Ka kidney chloride channels, *Br J Pharmacol* 160 (2010) 1652-1661.
- [37] A. Liantonio, A. Picollo, E. Babini, G. Carbonara, G. Fracchiolla, F. Loiodice, V. Tortorella, M. Pusch, D.C. Camerino, Activation and inhibition of kidney CLC-K chloride channels by fenamates, *Mol Pharmacol* 69 (2006) 165-173.
- [38] T.Y. Chen, Structure and function of clc channels, *Annu Rev Physiol* 67 (2005) 809-839.
- [39] G. Rickheit, H. Maier, N. Strenzke, C.E. Andreescu, C.I. De Zeeuw, A. Muenscher, A.A. Zdebik, T.J. Jentsch, Endocochlear potential depends on Cl⁻ channels: mechanism underlying deafness in Bartter syndrome IV, *Embo J* 27 (2008) 2907-2917.
- [40] S. Uchida, S. Sasaki. Function of chloride channels in the kidney, *Annu Rev Physiol* 67 (2005) 759-78.
- [41] N. Akizuki, S. Uchida, S. Sasaki, F. Marumo, Impaired solute accumulation in inner medulla of *Clcnk1*^{-/-} mice kidney, *Am J Physiol Renal Physiol* 280 (2001) F79-87.

FIGURE LEGENDS

Fig. 1. Activation of mClC-K1 channels by mBarttin. *A*, steady-state current-voltage relationships obtained in ND96 solution for non-injected oocytes and oocytes expressing mBarttin or mClC-K1 alone, mClC-K1/mBarttin and mClC-K1/Y95A mBarttin. Each data point represents the mean from at least 30 oocytes from three different batches; SEM is shown by an error bar when this is larger than the symbols. *B*, representative original voltage-clamp recordings obtained from oocytes expressing mBarttin or mClC-K1 alone, mClC-K1/mBarttin, mClC-K1/Y95A mBarttin, and from non-injected oocytes.

Fig. 2. Increase in the surface expression of mClC-K1 channels produced by mBarttin. Currents at +60 mV correspond to the same data as in Fig. 1A. The cell surface expression values (measured in RLU, relative light units) were normalized relative to those found for mClC-K1/Y95A mBarttin in the same batch of oocytes. Each column represents the mean from at least 30 oocytes for current recordings, and from at least 30 oocytes from three different batches of oocytes for the surface expression. SEM is shown as an error bar when larger than the symbols. *, statistical difference ($P < 0.05$) between mBarttin, mClC-K1, mClC-K1/mBarttin or mClC-K1/Y95A mBarttin vs non-injected oocytes.

Fig. 3. Electrophysiological properties of mClC-K1/Y95A mBarttin channels at the whole-cell level in *X. laevis* oocytes. *A*, selectivity towards different anions. Steady-state current-voltage relationships were obtained when 80 mM extracellular Cl^- was replaced by Br^- ($n = 15$), NO_3^- ($n = 11$) or Γ ($n = 35$). SEM is shown as an error bar when larger than the symbols. *B*, effects of changes in extracellular Ca^{2+} concentration or pH on mClC-K1/Barttin or mClC-K1 activity. Currents at +60 mV were normalized to those of control (pH 7.4, 1.5

mM Ca^{2+}). Each column represents the mean from at least 6 oocytes from three different batches of oocytes; SEM is shown as an error bar when larger than the symbols (different extracellular pH values, $n = 6-11$; different Ca^{2+} concentrations, $n = 6-11$). *, statistical difference ($P < 0.05$) in comparison to pH 7.4, 1 mM Ca^{2+} .

Fig. 4. mClC-K1/mBarttin single-channel recordings channels in *X. laevis* oocytes. *A*, Representative current trace recorded at a holding potential (V_{hold}) of -70 mV from an outside-out patch. The binned current amplitude histogram (shown below the traces) was used to determine the single channel current amplitude. The dotted line labeled *C* in this figure and subsequent figures denotes the closed current level. The current level at which all channels are closed was determined by visual inspection (the trace with the least electrical noise). “Full” and “half” single-channel current levels are indicated by 1 and $\frac{1}{2}$, respectively. *B*, Representative current traces recorded at different holding potentials from an experiment similar to that described in *A*. *C*, Average current-voltage relationships ($n = 5-11$) calculated from recordings similar to those shown in *B*. Open and closed circles represent “full” and “half” single-channel openings, respectively. Vertical bars represent SEM values. Binned current amplitude histograms (not shown for clarity) were used to determine the single-channel current amplitude (i) at each holding potential. The dashed line represents a Goldman-Hodgkin-Katz fit (GHK-fit) of the data for a Cl^- selective channel. Single-channel conductance was calculated from the GHK-fit of the average current-voltage relationships using the “Patch for Windows” program (written by Dr. B. Letz; HEKA Electronics GmbH, Germany).

Fig. 5. mClC-K1/mBarttin channel anion selectivity determined at the single-channel level in *X. laevis* oocytes *A, B*. Representative single-channel current recordings obtained at a holding potential (V_{hold}) of +50 mV from an outside-out patch. Bars above the traces indicate the presence of NaCl, NaI, or NaBr in the bath solution. The insets show segments of the same current traces on an expanded time scale. The segments correspond to the time intervals indicated by the black bars below the traces. The single-channel current amplitudes for Cl^- and Br^- (i_{Cl^-} and i_{Br^-} , respectively) were determined as described in Fig. 4. No detectable single-channel current events were observed in the trace when NaI was present in the bath.

Fig. 6. Whole-cell recordings of mClC-K1/mBarttin in HEK293-transfected cells. *A*, representative, original, whole-cell recordings obtained from cells expressing mClC-K1/mBarttin channels. The pipette was filled with 150 mM Cl^- . Cells were bathed in a solution at pH 7.4 or pH 9.0, or in a solution where 140 mM extracellular Cl^- was replaced by Γ . *B*, steady-state current-voltage relationships obtained from cells expressing mClC-K1/mBarttin channels under the same conditions as described in panel A (pH 7.4, $n = 7$; pH 9.0, $n = 4$; Γ , $n = 4$). *C*, steady-state current-voltage relationships obtained from cells expressing mClC-K1/mBarttin channels. Pipette was filled with 33 mM Cl^- . Cells were bathed in physiological saline solution at pH 7.4 ($n = 7$) or pH 9.0 ($n = 7$), or in a solution where 140 mM extracellular Cl^- was replaced by Γ ($n = 7$).

Fig. 7. mClC-K1 single-channel activity in HEK293-transfected cells. *A*, representative mClC-K1 current recordings in the cell-attached configuration obtained at various voltages for cells expressing mClC-K1 channels in the presence or absence of mBarttin. Binned current amplitude histograms for -85 mV membrane potential are shown below the traces. Cells were bathed in physiological saline solution, with high- Cl^- solution in the pipette. *B*,

current-voltage relationships in the cell-attached configuration for cells expressing mClC-K1 channels with ($n = 3-11$) or without mBarttin ($n = 4$), and in the inside-out configuration for cells expressing mClC-K1 channels with mBarttin ($n = 4-7$). Pipettes were filled with a high-Cl⁻ solution. SEM is shown as an error bar when larger than the symbols. *C*, channel voltage dependence in the cell-attached and in the inside-out configurations. Channel activity (*NPo*) is plotted against membrane voltage (*V_m*). Each point is the mean of 4-7 values for the cell-attached configuration, and of 5-6 values for the inside-out configuration. Pipettes were filled with high-Cl⁻ solution. SEM is shown as an error bar.

Fig. 8. Whole-cell recordings of V166E mClC-K1/mBarttin in HEK293-transfected cells. *A*, representative, original, whole-cell recordings. The pipette was filled with 150 mM Cl⁻. Cells were bathed in a solution at pH 7.4 or in a solution in which 140 mM extracellular Cl⁻ had been replaced by I⁻. *B*, steady-state current-voltage relationships under the same conditions as described in panel A (pH 7.4, $n = 12$; I⁻, $n = 14$).

Fig. 9. V166E mClC-K1 single-channel activity in cell-attached membrane patches from HEK293-transfected cells. *A*, representative V166E mClC-K1 current recordings obtained at various voltages for cells expressing mutant channels in the presence or in the absence of mBarttin. Binned current amplitude histograms for +85 mV membrane potential are shown below the traces. Cells were bathed in physiological saline solution, with a high-Cl⁻ solution in the pipette. *B*, current-voltage relationships for cells expressing mutant channels in the presence ($n = 3-4$) or in the absence ($n = 3-4$) of mBarttin. SEM is shown as an error bar when larger than symbols. *C*, channel voltage dependence. Channel activity (*NPo*) is plotted against membrane voltage (*V_m*). Each point is the mean of 3-4 values, with SEM shown as an error bar.

Characterization of the mouse CIC-K1/Barttin chloride channel ~~complex in the mouse~~

Sébastien L'Hoste^{a,b,c}, Alexei Diakov^d, Olga Andrini^{a,b,c}, Mathieu Genete^{a,b,c}, Laurent Pinelli^{a,b,c}, Teddy Grand^{a,b,c}, Mathilde Keck^{a,b,c}, Marc Paulais^{a,b,c}, Laurent Beck^e, Christoph Korbmacher^d, Jacques Teulon^{a,b,c}, and Stéphane Lourdel^{a,b,c}.

^aUPMC Univ Paris 06, UMRS 872, Laboratoire de génomique, physiologie et physiopathologie rénales, F-75005, Paris, France.

^bINSERM, UMRS 872, Laboratoire de génomique, physiologie et physiopathologie rénales, F-75005, Paris, France.

^cCNRS, ERL 7226, Laboratoire de génomique, physiologie et physiopathologie rénales, F-75005, Paris, France.

^dInstitut für Zelluläre und Molekulare Physiologie, Waldstr 6, 91054 Erlangen, Germany.

^eUniversité de Nantes, Faculté de Chirurgie dentaire, laboratoire d'ingénierie ostéoarticulaire et dentaire, Nantes, France

Corresponding author:

Stéphane Lourdel, UMRS 872, ERL 7226, Laboratoire de génomique, physiologie et physiopathologie rénales, 15 rue de l'Ecole de Médecine, 75270 Paris cedex 06, France

Phone: 33.1.55.42.78.55

Fax: 33.1.46.33.41.72

E-mail: stephane.lourdel@upmc.fr

ABSTRACT

Several Cl⁻ channels have been described in the native renal tubule, but their correspondence with ClC-K1 and ClC-K2 channels (orthologs of human ClC-Ka and ClC-Kb), which play a major role in transcellular Cl⁻ absorption in the kidney, has yet to be established. This is partly because investigation of heterologous expression has involved rat or human ClC-K models, whereas characterization of the native renal tubule has been done in mice. Here, we investigate the electrophysiological properties of mouse ClC-K1 channels heterologously expressed in *Xenopus laevis* oocytes and in HEK293 cells with or without their accessory Barttin subunit. Current amplitudes and plasma membrane insertion of mouse ClC-K1 were enhanced by Barttin. External basic pH or elevated calcium stimulated currents followed the anion permeability sequence Cl⁻ > Br⁻ > NO₃⁻ > I⁻. Single-channel recordings revealed a unit conductance of ~40 pS. Channel activity in cell-attached patches increased with membrane depolarization (voltage for half-maximal activation: ~ -65 mV). Insertion of the V166E mutation, which introduces a glutamate in mouse ClC-K1, which is crucial for channel gating, reduced the unit conductance to ~20 pS. This mutation shifted the depolarizing voltage for half-maximal channel activation to ~ +25 mV. The unit conductance and voltage dependence of wild-type and V166E ClC-K1 were not affected by Barttin. Owing to their strikingly similar properties, we propose that the ClC-K1/Barttin complex is the molecular substrate of a chloride channel previously detected in ~~the present study in intercalated cells of the mouse outer medullary collecting duct, and previously in~~ the mouse thick ascending limb ([Paulais et al., J Membr. Biol, 1990, 113:253-260](#)).

KEYWORDS

Chloride channel, ClC, kidney, ClC-K1, patch-clamp

NON-STANDARD ABBREVIATIONS

CCD: cortical collecting duct

ClC-K: kidney chloride channel

CNT: connecting tubule

CTAL: cortical thick ascending limb

DCT: distal convoluted tubule

DIDS: 4,4'-diisothiocyanato-2,2'-stilbene disulfonic acid disodium salt

DPC: 2-(phenylamino) benzoic acid

NPPB: 5-nitro-2-(3-phenylpropylamino) benzoic acid

OMCD: outer medullary collecting duct

1. INTRODUCTION

Two Cl⁻ channels of the ClC family, ClC-K1 and ClC-K2 (or their human orthologs ClC-Ka and ClC-Kb, respectively), play a pivotal role in transcellular Cl⁻ absorption in the kidney. Located on the basolateral membrane, they are present throughout the distal nephron [1-3], but the specific distribution of each ClC-K is still uncertain owing to the lack of isoform-specific antibodies [4]. Mutations in human genes coding for ClC-Kb and the regulatory subunit, Barttin, are responsible for salt-losing tubulopathies, namely Bartter's syndrome types 3 and 4, respectively [5-7]. Rare types of Bartter's syndrome can also result from compound mutations in ClC-Kb and ClC-Ka [8]. Renal function has not been investigated in knockout mice for ClC-K2 because they die very early; ClC-K1-knockout mice display impaired urine concentration and nephrogenic diabetes insipidus [9]. In accordance with pathological and physiological data, localization studies suggest that ClC-K2 is highly expressed in the cortical part of the distal nephron, and that ClC-K1 is mostly restricted to the medullary part of the renal tubule [2, 3, 10, 11].

The functional expression of human and rat ClC-K remained controversial until their accessory subunit, Barttin, was identified. It promotes their insertion into the plasma membrane [2, 12]. This discovery made it possible to identify two fundamental properties of ClC-K channels. First, the relative permeability for anions follows the sequence Cl⁻ > Br⁻ > NO₃⁻ > I⁻ for ClC-Ka, and Cl⁻ > Br⁻ = NO₃⁻ > I⁻ for ClC-Kb; second, the currents are enhanced by a basic external pH and high external calcium concentrations [2, 12]. Interestingly, a glutamate residue that plays a critical role in the protopore gating of other ClC chloride channels is missing in ClC-K channels, where it is replaced by a valine. For this reason, it has been suggested that the two protopores in ClC-K dimers are constitutively open. Thus, the common gate (involving both subunits of the dimers) may act as the major regulator of ClC-K

channels. In recent studies on rat ClC-K1, Fahlke's group reintroduced the "gating" glutamate and observed profound effects on both conductance and gating [4, 13, 14].

We and others have identified several basolateral chloride channels in different parts of the renal tubule, particularly in the cortical thick ascending limb (CTAL), the distal convoluted tubule (DCT), the connecting tubule (CNT), and the cortical collecting duct (CCD) [15-23]. Two of these channels, with conductances of 45 pS and 9 pS, respectively, display properties that are compatible with those of ClC-K chloride channels [24].

Nevertheless, the precise molecular identity of these channels remains elusive, because heterologous expression data are incomplete and heterogeneous. Studies of recombinant channels have involved rat and human ClC-Ks, whereas most of those of the native renal tubule have involved mouse kidney. Furthermore, there are only a few single-channel recordings available for recombinant channels, and they all derive from studies on human ClC-Ka and rat ClC-K1 [4]. In this study, we investigated the properties of recombinant mouse ClC-K1 channels expressed in the presence or absence of mouse Barttin, in an attempt to establish a coherent basis for their correspondence with native chloride channels in the mouse renal tubule.

2. MATERIAL AND METHODS

~~2.1. Mice~~

~~The animals used in this study were handled in full compliance with the French government welfare policy. This work was performed under Permit No 75-1416 from the Veterinary Department of the French Ministry of Agriculture.~~

2.1. Molecular biology

The mouse CIC-K1 cDNA clone (image 5042736, Invitrogen, Carlsbad, CA, USA) and mouse Barttin (a generous gift from Prof. T. J. Jentsch, MDC/FMP, Berlin, Germany) were subcloned into pSP64-S and pVITRO2 vectors, respectively, for expression in *Xenopus laevis* oocytes. Capped cRNAs were synthesized *in vitro* from wild-type and mutant CIC-K1 and Barttin vectors using the SP6 mMessage mMachin Kit (Ambion, Austin, TX, USA). To evaluate the surface expression of CIC-K1 in *Xenopus laevis* oocytes, we externally tagged CIC-K1 by introducing a FLAG epitope (DYKDDDDK) between transmembrane domains L and M (beginning at position 377). This did not interfere with their ability to generate currents.

For electrophysiological recordings, HEK293 cells were cotransfected with 1 µg of a bicistronic vector pVITRO2 containing the coding sequence of mouse CIC-K1 and mouse Barttin, and 0.3 µg of a IRES vector encoding the CD8 antigen (a generous gift from Dr. J. Barhanin, Université Nice Sophia Antipolis, Nice, France) as a transfection marker by electroporation or using X-tremeGENE9 (Roche Diagnostics, Meylan, France). Including CD8 made it possible to identify the transfected cells using anti-CD8-coated beads (Invitrogen Dynal, Oslo, Norway). Site-directed mutagenesis was performed with the Quickchange site-directed mutagenesis kit (Stratagene, La Jolla, CA, USA).

All constructs were fully sequenced.

2.2. Two-electrode voltage-clamp

Defolliculated *Xenopus laevis* oocytes were injected with 10 ng of ClC-K1 cRNA and 5 ng of Barttin cRNA. The oocytes were then kept at 17°C in modified Barth's solution containing (in mM): 88 NaCl, 1 KCl, 0.41 CaCl₂, 0.32 Ca(NO₃)₂, 0.82 MgSO₄, 10 HEPES, pH 7.4, and supplemented with gentamycin (20 µg/ml). Three days after injection, two-electrode voltage-clamp experiments were performed using a TEV-200A amplifier (Dagan, Minneapolis, MN, USA) and PClamp 9 software (Molecular Devices, Sunnyvale, CA). Pipettes were made from borosilicate tubes (GC150T, Harvard Apparatus, Edenbridge, UK), and filled with 3 M KCl. Currents were recorded in ND96 solution containing (in mM): 96 NaCl, 2 KCl, 1.5 CaCl₂, 1 MgCl₂, 5 HEPES, pH 7.4. Currents were recorded in response to a voltage protocol consisting of 20 mV steps from -160 mV to +100 mV with a duration of 800 ms from a holding potential of -30 mV. The data were filtered at 300 Hz, and sampled using a Digidata 1320A analogue-to-digital converter (Molecular Devices, Sunnyvale, CA).

For anion replacement, 80 mM Cl⁻ was replaced by equivalent amounts of Br⁻, I⁻ or NO₃⁻. HEPES was replaced by equimolar MES for solutions at pH 5.4-6.4, or by Tris for solutions at pH 8.4. Where appropriate, calcium acetate was added to the ND96 solution to increase the extracellular calcium concentration. The permeability ratios of various anions (X⁻) relative to that of Cl⁻ (P_{X^-}/P_{Cl^-}) were calculated using the modified Goldman-Hodgkin-Katz equation [25]:

$$\frac{P_{X^-}}{P_{Cl^-}} = \frac{(104 \times e^{40 \times (E_1 - E_2) - 24})}{80}$$

Where E_1 and E_2 are the reversal potentials for Cl⁻ and X⁻, respectively.

Chloride channel inhibitors were purchased from Sigma-Aldrich (Saint-Quentin Fallavier, France). DPC, at a concentration of 0.5 M, and NPPB, at a concentration of 0.1 M, were dissolved in DMSO. DMSO (at the maximum concentration of 0.2% used for 10^{-3} M DPC) had no effect on channel activity.

2.3. Whole-cell recording

HEK293 cells were transiently transfected by electroporation, and plated on 35-mm plastic Petri culture dishes. 20 h after transfection, the Petri dishes were mounted on the inverted stage of a microscope. The bath solution contained (in mM): 140 NaCl, 2 CaCl₂, 1 MgCl₂, 22 Sucrose, 10 HEPES, pH 7.4. HEPES was replaced by TRIS for solutions at pH 9.0. For the chloride substitution experiments, 140 NaCl was replaced by 140 NaI. The pipette solution contained (in mM): 150 NMDG-Cl, 1 MgCl₂, 2 EGTA, 1 Mg-ATP, 10 HEPES, pH 7.4 or 33 CsCl, 100 NaGluconate, 1 MgCl₂, 2 EGTA, 1 Mg-ATP, and 10 HEPES, pH 7.0. Standard whole-cell recordings were performed using an Axopatch 200B (Molecular Devices, Sunnyvale, CA) and PClamp 9 software (Molecular Devices, Sunnyvale, CA). The bath was earthed *via* an agar 3 M agar bridge. Patch-clamp pipettes had resistances of 2-3 MΩ. The following pulse protocol was used: from a holding potential of -30 mV, after a pre-pulse to +65 mV for 30 ms, voltage was stepped from -115 mV to +105 mV in 20 mV increments for 160 ms, and followed by a pulse to +105 mV.

2.4. Single-channel recordings in outside-out patches of *Xenopus laevis* oocytes

Recordings in outside-out membrane patches of mCIC-K1 and mBarttin expressing oocytes were performed essentially as described previously using a conventional patch-clamp technique [26, 27]. Patch pipettes were pulled from borosilicate glass capillaries, and had a tip diameter of about 1-1.5 μm after fire polishing. Pipettes were filled with the KCl pipette

solution (in mM: 55 KCl, 35 K-gluconate, 5 NaCl, 1.2 MgCl₂, 2 EGTA, 10 HEPES, pH 7.28). Seals were routinely formed in a low sodium NMDG-Cl bath solution (in mM: 95 NMDG-Cl, 1 NaCl, 4 KCl, 1 MgCl₂, 1 CaCl₂, 10 HEPES, pH 7.4). In the NaCl bath solution, 95 mM NMDG-Cl was replaced by 95 mM NaCl. In the NaBr, NaI and NaNO₃ bath solutions, 95 mM NMDG-Cl was replaced by 10 mM NaCl and by 85 mM NaBr, 85 mM NaI and 85 mM NaNO₃, respectively. After seal formation, the bath solution was changed to the NaCl, NaI, NaBr or NaNO₃ bath solutions. Single-channel current data were initially filtered at 3 kHz and sampled at 9 kHz. Current traces were re-filtered at 250 Hz to resolve the single channel current amplitude (*i*).

2.5. Single-channel recordings in HEK293 cells ~~and OMCD tubules~~

HEK293 cells were transiently transfected using X-tremeGENE9 according to the Manufacturer's instructions (Roche Diagnostics, Meylan, France). Recordings were performed two days after transfection. The cells were initially bathed in physiological saline containing (in mM): 140 NaCl, 5 KCl, 1 CaCl₂, 1 MgCl₂, 10 glucose, 10 HEPES, pH 7.4.

~~Recordings on mouse OMCD were done essentially as previously described [23]. Briefly, OMCD segments were microdissected from collagenase treated kidneys, transferred into a Petri dish, and bathed in physiological saline.~~

The pipettes made from borosilicate tubes (GC150T, Harvard Apparatus, Edenbridge, Kent) were coated with Sylgard (Dow Corning, Seneffe, Belgium), and polished just before use. The pipettes were filled with a high-Cl⁻ solution containing (in mM): 150 NMDG-Cl, 1 MgCl₂, 10 glucose, and 10 HEPES, pH 7.4. The solutions used to characterize channel properties in the inside-out configuration contained 2 mM EGTA and no calcium. To record the currents, we used a RK 400 patch-clamp amplifier (Bio-logic, Claix, France) and PClamp 9 software (Molecular Devices, Sunnyvale, CA). Currents were filtered at 300 or 500 Hz, and

were sampled at 1-2 kHz using a Digidata 1322A analogue-to-digital converter (Molecular Devices, Sunnyvale, CA). The mean current (I) passing through N channels was used to calculate the normalized current (NPo) according to the equation $NPo=I/i$, where i is the unitary current amplitude. The relationship between NPo and voltage (V) was fitted using a Boltzmann equation:

$$NPo(V) = NPo_{\min} + \frac{NPo_{\max} - NPo_{\min}}{1 + \exp((V_{1/2} - V)/k)}$$

where V is the membrane voltage, NPo_{\min} and NPo_{\max} are the minimum and maximum values of NPo , respectively, $V_{1/2}$ is the half-maximal activation voltage, and k is the slope factor of the voltage dependence. The liquid junction potentials were calculated with PClamp 9 and corrected accordingly.

2.6. Measurement of surface expression

Experiments were performed as previously described [28], using an anti-FLAG M2 monoclonal antibody (Sigma-Aldrich, St. Louis, MO, USA) as the primary antibody, and a peroxidase-conjugated goat anti-mouse antibody (Santa Cruz Biotechnology Inc., Santa Cruz, CA, USA) as the secondary antibody. Chemiluminescence was quantified in a Turner TD-20/20 luminometer (Turner Designs, Sunnyvale, CA, USA) by placing individual oocytes in 50 μ l of SuperSignal Elisa Femto Maximum Sensitivity Substrate Solution (Pierce, Rockford, IL, USA).

2.7. Statistics

Results are shown as mean \pm SEM. n indicates the number of experiments. Statistical significance was determined by a paired Student's t -test using SigmaStat software (SPSS, Erkrath, Germany). A value of $P < 0.05$ was considered to be significant.

3. RESULTS

3.1. Functional characterization of mClC-K1 channels at the whole-cell level in *X. laevis* oocytes

We expressed mouse ClC-K1 channels (mClC-K1) in *X. laevis* oocytes, with or without mouse Barttin (mBarttin), to characterize their conductive properties at the whole cell level. As previously reported for rat ClC-K1 (rClC-K1) [12, 25, 29], mClC-K1 alone induced small but significant currents, while co-expression with mBarttin markedly increased the current intensity ($n = 30$; Fig. 1A, B). In human Barttin, mutation of a putative proline-tyrosine (PY) motif (Y98A) further enhances hClC-K currents [2]. Likewise, mClC-K1 currents were also greater in oocytes expressing mBarttin mutated at the equivalent position (Y95A) than in oocytes expressing non-mutated Barttin ($n = 30$; Fig. 1A, B). mBarttin and Y95A mBarttin alone produced currents that were not different from those in non-injected oocytes ($n = 30$; Fig. 1A, B). There was a time-dependent increase in the mClC-K1 current at the highest positive voltages, and the corresponding current/voltage relationships showed outward rectification (Fig. 1B), which was reminiscent of hClC-Kb, rather than of hClC-Ka or rClC-K1, which display linear or slightly inwardly rectifying currents [2, 12].

Using a chemiluminescence assay and taking advantage of the extracellular FLAG-tag placed on mClC-K1, we observed that mBarttin and Y95A mBarttin increased plasma membrane expression of ClC-K1 by ~177% ($n = 30$) and ~393% ($n = 30$), respectively (Fig. 2). Since surface expression correlated with channel currents (Fig. 2), the significant increase in current amplitudes of mClC-K1 channels could be ascribed to increased surface expression by mBarttin.

We then investigated the key electrophysiological properties of mClC-K1 in oocytes injected with the Y95A mBarttin mutant. We first assessed the selectivity among anions from

current-voltage measurements when most of the Cl^- in the bathing solution (80 mM) had been replaced by the test anion (Fig. 3A). The analysis of the data yielded $P_{\text{I}^-}/P_{\text{Cl}^-} = 0.20 \pm 0.05$ ($n = 35$), $P_{\text{NO}_3^-}/P_{\text{Cl}^-} = 0.35 \pm 0.18$ ($n = 11$), and $P_{\text{Br}^-}/P_{\text{Cl}^-} = 0.86 \pm 0.14$ ($n = 15$). This indicates a permeability sequence of $\text{Cl}^- > \text{Br}^- > \text{NO}_3^- > \text{I}^-$, which is similar to that observed previously for rClC-K1, for hClC-Ka [2, 12, 25], and for the Cl^- channel in the basolateral membrane of mouse CTAL [19].

Also consistently with previous results [2, 12, 25, 30], we found that the currents elicited by mClC-K1/Y95A mBarttin channels decreased by $65 \pm 1\%$ ($n = 6$) in response to extracellular acidification (pH 6.0), and by $50 \pm 1\%$ ($n = 6$) in response to the removal of extracellular calcium (Fig. 3B). They increased by $55 \pm 9\%$ ($n = 9$) at pH 8.0 and by $76 \pm 6\%$ ($n = 6$) in the presence of 5 mM of extracellular calcium (Fig. 3B). [Similar results were obtained in the absence of mBarttin \(Fig. 3B\) \(\$n = 11\$ \).](#)

We investigated the effects of several classical Cl^- channel blockers by adding them to the extracellular solution. At +60 mV, DIDS (100 μM) reduced mClC-K1/Y95A mBarttin currents by $53 \pm 1\%$ ($n = 6$) (not shown). Both DPC (1 mM) and NPPB (100 μM) blocked the channels to a lesser extent, reducing currents by $34 \pm 1\%$ ($n = 6$) and $42 \pm 1\%$ ($n = 6$), respectively (not shown). Qualitatively similar results have been obtained on rClC-K1 [25, 29 31], except for DPC, the effect of which is particularly tenuous as far as mClC-K1 is concerned.

[Taking these results as a whole, mClC-K1 displays the major hallmarks of recombinant ClC-K1 channels, including \$\text{Cl}^- > \text{Br}^- > \text{NO}_3^- > \text{I}^-\$ anion selectivity, sensitivity to external pH and calcium, and increased expression at the membrane with Barttin. In addition, the anion selectivity sequence is identical to that found by Paulais et al. \[19\] for the 45-pS native \$\text{Cl}^-\$ channel, and slightly different from that found for the 9-pS channel \[21, 22, 23\].](#)

3.2. Single-channel recordings of mCIC-K1 channels in *X. laevis* oocytes

To investigate the single-channel properties of mCIC-K1/mBarttin heterologously expressed in *Xenopus laevis* oocytes, we performed outside-out patch clamp experiments essentially as previously described [26, 27]. Fig. 4A shows a representative single-channel current trace recorded at a holding potential of -70 mV. The corresponding binned current amplitude histogram is shown below the current trace. These data indicate that single-channel events with two different current amplitudes can be detected, as expected, for a double-barrelled channel of the CIC ion channel family [32-34]. In similar recordings, single-channel current amplitude of events with “full” and “half” openings averaged -1.9 ± 0.08 pA ($n = 11$) and -0.98 ± 0.04 pA ($n = 11$), respectively.

Fig. 4B shows representative, single-channel, current traces recorded at different holding potentials in an outside-out patch from another oocyte also expressing mCIC-K1/mBarttin channels. Fig. 4C shows averaged current/voltage relationships ($n = 5-11$) obtained from similar recordings as shown in Fig. 4B. These data demonstrate that mCIC-K1/mBarttin channels has single-channel “full” and “half” conductances of 44.9 ± 1.4 pS ($n = 12$) and 23.9 ± 0.9 pS ($n = 12$), respectively. The anion selectivity of mCIC-K1 expressed in oocytes, when assessed at the single-channel level, was compatible with that measured using voltage-clamp whole-cell recordings. This is illustrated by the representative single-channel current traces shown in Fig. 5 (holding potential: $+50$ mV). At this potential, with Γ in the bath solution, no single-channel event was detected (Fig. 5A). With Br^- in the bath, the “full” and “half” single-channel current amplitudes (i_{Br^-} : 1.3 and 0.65 pA, respectively) were ~46% lower than the same currents in the presence of Cl^- (i_{Cl^-} : 2.3 and 1.25 pA, respectively) (Fig. 5B). Similar observations were made in a total of 5 experiments.

The unit conductance of mCIC-K1, as assessed in the oocyte expression system, is compatible with that of the native 45-pS Cl^- channel [19].

3.3. Whole-cell recordings of mCIC-K1 channels in HEK293 cells

Whole-cell current recordings were conducted in HEK293 cells, and revealed linear currents when the pipette was filled with 150 mM Cl⁻ ($n = 4$) (Fig. 6A, B). The whole-cell currents were in the same range as the rat CIC-K1 currents recorded previously by Scholl *et al.* [13]. They were significantly increased by elevating the extracellular pH to 9.0 ($n = 4$), and were significantly reduced by the partial replacement of extracellular Cl⁻ by I⁻ ($n = 4$) [2, 12, 25, 30]. In contrast to what is observed in the oocyte expression system, no time-dependent relaxation components were visible on the current traces (Fig. 6A). That the shape of the currents depended on the expression system had also been noted previously for CIC-Ka and CIC-Kb [4]. CIC-Ka also exhibits a linear current-voltage relationship with 150 mM Cl⁻ in the pipette, while rCIC-K1 is inwardly rectifying [13, 14]. This difference might be attributable to the fact that rCIC-K1, which is clearly voltage-dependent when transfected in cultured cells, is activated in response to hyperpolarization [13, 14, 35]. For mCIC-K1, the current/voltage relationships (Fig. 6C) showed outward rectification in the presence of a low internal Cl⁻ solution (35 mM) ($n = 7$).

These results suggest that HEK293 cells is a suitable model for studying mCIC-K1 currents at the single-channel level.

3.4. Conductive properties of mCIC-K1 channels at the single-channel level in HEK293 cells

Fig. 7A shows typical recordings of mCIC-K1/mBarttin channel activity on cell-attached membrane patches from HEK293-transfected cells bathed with physiological saline solution, with the pipette filled with a high-Cl⁻ solution. Under these conditions, we observed highly active channels (Fig. 7A). It is apparent that most mCIC-K1 channels displayed “full” opening when expressed in HEK293 cells. The current/voltage relationship displayed rather marked outward rectification, probably due to low [Cl⁻]_i (Fig. 7B). The unit conductance of

the “full” openings, measured in the linear part of the current-voltage relationship, averaged 41.9 ± 1.5 pS ($n = 11$). The reversal potential (-1.8 ± 1.2 mV, $n = 11$) was close to zero. Fig. 7B also shows the linear current/voltage relationship obtained in the inside-out configuration when high-Cl⁻ solutions were present on both sides of the membrane patch. The unit conductance (44.4 ± 1.4 pS, $n = 7$) was not statistically different from that determined in the cell-attached configuration.

Channel activity increased at positive potentials (Fig. 7A). This was typically observed in 7 cell-attached patches, in which we investigated the voltage dependence of the *NPO*. The mean relationship between *NPO* and voltage is given in Fig. 7C. Fitting our data with a Boltzmann equation yielded a half-maximal activation voltage ($V_{1/2}$) of -65.6 mV. Voltage dependence was no longer observed in the inside-out configuration, suggesting that it is mediated by some intracellular factor (Fig. 7C).

To investigate the possible modulation of mClC-K1 channel gating and unit conductance by mBarttin [13, 14], we performed single-channel analysis in cell-attached membrane patches using HEK293-transfected cells expressing mClC-K1 alone. Fig. 7B and Fig 7C show that neither the unit conductance (38.1 ± 1.4 pS; $n = 4$) nor the voltage dependent activation of the channel ($V_{1/2} = -70.1$ mV) were significantly modified compared to mClC-K1 co-expressed with Barttin.

These results, as a whole, show that the single-channel properties of mClC-K1/mBarttin are strikingly similar to those of the 45-pS native Cl⁻ channel [19]. In particular, the open probability has values close to those measured in the mouse CTAL [19] when measured on HEK293 cells.

3.5. Conductive properties of V166E mCIC-K1 mutant channels in HEK293 cells

We anticipated that introducing a glutamate at a position equivalent to 166 might create a protopore gate, making it easier to detect the openings of the protopores. In CIC-0, changes in the amino acid at the equivalent position 166 did not alter the protopore conductance [34]. In a first step, we performed whole-cell recordings in HEK293 cells using 150 mM Cl⁻ in the pipette solution (Fig. 8). The V166E mutant displayed clear outward rectification under these conditions suggesting that the gating of the channel has been modified in agreement with our hypothesis.

Fig. 9A shows representative cell-attached current recordings from HEK-293 cells transfected with V166E mCIC-K1/mBarttin channels. The mean current-voltage relationship was essentially linear (Fig. 8B) and reversed at -1.4 ± 2.1 mV; a unit conductance of 19.9 ± 1.3 pS was computed ($n = 4$). Channel activity increased at positive voltages ($n = 4$) (Fig. 8C). The best fit of our data indicated that the half-maximal activation voltage of the mutant channel was shifted to more positive potentials as compared to WT mCIC-K1/mBarttin ($V_{1/2} = 24.9$ mV). Voltage dependence persisted in the cell-free mode (not shown). In contrast, two other point mutations introduced at position 166 did not have the same effect as V166E. The V166L mutation did not significantly modify the unit conductance (38.5 ± 4.0 pS, $n = 3$; not shown), and the V166M only moderately modified the unit conductance (38.5 and 29.5 pS, $n = 2$; not shown). We can therefore reasonably conclude that the V166E mutation revealed the activity of the channel protopore by introducing *de novo* protopore gating.

We also recorded single-channel activity from cell-attached patches from HEK-293 cells transfected with V166E mCIC-K1 without mBarttin: there was no significant change in unit conductance (18.3 ± 0.7 pS; $n = 4$) (Fig. 9B), channel voltage dependence ($n = 4$) (Fig. 9C), or for half-maximal voltage activation ($V_{1/2} = 21.7$ mV).

3.6. There is a similar channel in the basolateral membranes of intercalated cells of mouse OMCD

Previous studies have characterized a chloride channel with properties similar to mCIC-K1 in the basolateral membrane of mouse CTAL [19], but not in other parts of the cortical distal nephron [24]. Since immunofluorescence studies have indicated that Barttin and CIC-K1/CIC-K2 channels were present downwards in the medulla [1, 2, 32], we searched for Cl⁻ channels in the intercalated cells of the outer medullary collecting duct. Using NMDG-Cl⁻ solutions in the pipette, we were able to record a small channel with properties similar to those previously reported for the 9 pS chloride channel [21-23] (not shown) together with a higher conductance channel. Representative current traces recorded at different holding potentials are shown in Fig. 9A. The unit conductance measured on cell-attached patches was 37.4 ± 4.2 pS ($n = 7$) (Fig. 9B). The activity of the channel was dependent on the external calcium concentration: we recorded 1.8 ± 0.2 channels per patch in the presence of 1 mM Ca²⁺ ($n = 5$) and 6.7 ± 0.9 in the presence of 5 mM Ca²⁺ ($n = 3$, $p < 0.05$) in the pipette. We were unable to record any channel activity in the cell-free configuration.

4. DISCUSSION

4.1. The apparent properties of mClC-K1 partly depend on the heterologous expression model

Fahlke & Fischer [4] have previously pointed out that there are clear kinetic and current/voltage relationships differences between ClC-K channels expressed in *X. laevis* oocytes and those expressed in mammalian cells. This was also observed for the mouse ClC-K1, but can be partly explained by the differing experimental conditions.

In HEK293 cells, mClC-K1/mBarttin yields linear currents with 150 mM Cl⁻ in the pipette and outwardly rectifying currents in the presence of low Cl⁻ (35 mM), a situation closer to that seen in the oocytes. Indeed, in *X. laevis* oocytes where the intracellular Cl⁻ is around 30-50 mM, currents are outwardly rectifying. Furthermore, single-channel current amplitudes in the cell attached mode also showed outward rectification (low intracellular Cl⁻ concentration). We can therefore assume that the discrepancy in the shapes of the current/voltage relationships obtained for whole-cell currents between heterologous expression models is due to normal, Goldman-type rectification, and is related to the level of intracellular chloride.

The time-dependent components that increase mClC-K1 currents at positive voltages in *X. laevis* oocytes suggest activation at depolarizing voltages, which was not observed in whole-cell recordings from HEK293 cells. However, the NP_o of the mClC-K1 increased in response to depolarization in cell-attached patches from HEK293 cells, a condition in which the cell is intact (as for oocyte recordings). We may speculate that cell dialysis during whole-cell recording removed some component necessary for voltage gating. Indeed, the voltage-dependence that was observed in cell-attached patches also disappeared in inside-out patches.

In contrast to cell-attached recordings of HEK 293 cells, recordings from outside-out patches from oocytes always displayed very low open probability. A very low open

probability has also been observed when recording ClC-Ka from cell-free patches obtained on oocytes [36]. In contrast, ClC-Ka single-channel activity recorded from patches attached to mammalian cultured cells is high (see for instance, [14]). It may be speculated that, for some unknown reason, the mClC-K1 channels experience rundown following excision. Overall, mClC-K1/Barttin expressed in HEK293 cells more faithfully reflects the native 45-pS Cl channel.

4.2. The properties of mouse ClC-K1 are comparable to those of recombinant human ClC-Ka and rat ClC-K1

So far, only the electrophysiological properties of human and rat ClC-K channels have been investigated. Previous studies have demonstrated that recombinant hClC-Ka and rClC-K1 have identical properties at the whole-cell level in terms of anion selectivity, sensitivity to external pH and Ca^{2+} , and sensitivity to chloride channels blockers as DIDS and NPPB [2, 12, 25, 30, 31, 37]. However, rClC-K1 channels are active in the absence of Barttin; whereas hClC-Ka channels need Barttin to become anion conductive at the cell surface [2, 12, 30]. Our findings provide evidence that mClC-K1 shares many of the properties of hClC-Ka and rClC-K1 at the whole cell level, including the anion selectivity sequence ($\text{Cl}^- > \text{Br}^- > \text{NO}_3^- > \text{I}^-$), being activated at external basic pH or elevated Ca^{2+} , and sensitivity to DIDS and NPPB.

We also observed that mClC-K1, like rClC-K1, is active without mBarttin. There are also small differences that concern the voltage dependence (activation by depolarization for mClC-K1, by hyperpolarization for rat ClC-K1) and unitary conductances (40 pS for mClC-K1, 33 pS for rClC-K1 and 26 pS for hClC-Ka) [13, 14].

4.3. Single-channel activity in HEK293 cells reflects dimer gating of mCIC-K1

CIC channels, which function as dimer complexes, are endowed with two voltage-dependent gates, the protopore (“fast”) gate, and the common (“slow”) gate [38]. Protopore gating requires the presence of a glutamate at equivalent position 166. Indeed, substituting glutamate for valine (or alanine) in CIC-0 abolishes most of the protopore gating, and only brief closures of the protopores are detected [34]. Since the CIC-K channels have a valine residue at position 166 rather than a glutamate, it may be anticipated that their voltage dependence is due to common gating. Accordingly, the experiments we performed in the cell-attached mode in HEK293 transfected cells showed that half openings and closings of mCIC-K1 due to protopore gating were rarely detected in these recordings. As a consequence, the NP_o values found in these experiments essentially reflect the activity of the common gate.

Thus, the common gate of mCIC-K1 channels is moderately activated by depolarization. It is noteworthy that the half-maximal activation voltage $V_{1/2}$ (~ -65 mV), which is close to the resting membrane potential in renal cells, suggests that this regulation might be physiologically relevant. In sharp contrast, rCIC-K1 channels are activated by hyperpolarization [13, 14]. In this case, the voltage dependence is due to the fast gate, the slow gate being voltage-independent [14]. This may indicate that CIC-K regulation differs in different species. It could also indicate that the protopore gate, which according to Fahlke et al. [13, 14] is activated by hyperpolarization, might contribute to the total open probability, notably under physiological circumstances that were not encountered in our experiments.

4.4. Barttin has no influence on CIC-K1 channel gating or conductance

Barttin is an accessory regulatory subunit that is essential for the functional expression of hCIC-Ka and hCIC-Kb, and which also increases the current generated by rCIC-K1 [14]. We also observed that mCIC-K1 currents were greater in the presence of Barttin. However,

mCIC-K1, like rCIC-K1, carried currents in the absence of Barttin when expressed in heterologous expression systems. Furthermore, we observed that mCIC-K1 currents were still stimulated by external calcium and inhibited by protons in the absence of Barttin. Consequently, this must be an intrinsic property of the CIC-K, as has been reported elsewhere [12].

Barttin also modulates CIC-K gating [14]. Fahlke et al. initially reported that rCIC-K1 was activated by hyperpolarization in both the presence and the absence of Barttin [13]. Later on, however, they reported that the voltage dependence of rCIC-K1 expressed alone was not voltage dependent [14]. In the absence of Barttin, V166E rCIC-K1 channels were activated by membrane hyperpolarization, whereas in the presence of Barttin, mutant CIC-K1 channels were activated by membrane depolarization [13, 14]. In the present study, the voltage dependence of wild-type and V166E mCIC-K1 channels was not modified in the absence of Barttin.

Thus, the main effect of Barttin is to increase the number of mCIC-K1 channels in the plasma membrane. However, the fact that mCIC-K1, like rCIC-K1, is active in the absence of Barttin raises questions about the physiological role of this accessory subunit. The observation that Barttin-knockout mice suffer from severe renal salt and water loss, and die within a few days after birth demonstrates that Barttin is strictly necessary for CIC-K function in mouse kidneys [39]. There are two possible explanations. First, in the absence of Barttin, the expression of CIC-K1 at the plasma membrane is insufficient to sustain sufficient chloride transport. A possible alternative explanation, although the two are not mutually exclusive, could be that Barttin is required for CIC-K1 to be addressed specifically to the basolateral membrane. Indeed, some mutations of *BSND* result in the increased expression of CIC-Kb at the apical membrane [35].

4.5. ~~Comparison with native Cl⁻ channels in the mouse renal tubule~~ mClC-K1 underlies the native 45-pS chloride channel

Several chloride channels have been identified in the basolateral membranes of microdissected mouse renal tubules by means of single-channel recordings.

The first Cl⁻ channel we reported in mouse CTAL had a unit conductance of 45 pS, and a permeability sequence Cl⁻ > Br⁻ > NO₃⁻ [19]. No current was recorded in the presence of I⁻, suggesting that this anion has a blocking effect. Importantly, this channel was activated by depolarization, a property that disappeared after excision of the membrane patch. ~~All these properties are similar to those of mClC-K1. Thus, the 45 pS chloride channel that we have characterized in the basolateral membrane of mouse CTAL most likely corresponds to mClC-K1. In the present study, we also recorded a similar channel in the intercalated cells of the mouse OMCD, and showed that the activity of the channel was stimulated by external calcium.~~

~~A second Cl⁻ channel has been detected throughout the length of the distal nephron [21-23]. It has a conductance of 9 pS. We have previously suggested that it is underpinned by ClC-K2 on the basis of its anion selectivity sequence and the fact that it is distributed throughout the renal tubule [24]. This remains to be directly proved, since recombinant ClC-K2 has not so far been studied at the single-channel level. Finally, we should mention that a third Cl⁻ channel has been reported, the properties of which are incompatible with those of the ClC-Ks [20, 24]~~

4.6. Physiological roles of ClC-K1

Initially, ClC-K1 expression was thought to be restricted to the thin ascending limb [30], where it provides a transcellular route for Cl⁻ absorption, while Na⁺ follows via the

paracellular pathway [40]. Due to this strategic localization, CIC-K1 was believed to play a major role in urine concentration [9, 40].

The current view, however, proposes that CIC-K1 is more widely distributed along the renal tubule than previously thought [2, 3, 12]. In particular, it is also present in the MTAL and CTAL, where we have detected its single-channel properties [19]. This segment absorbs 25% of filtered NaCl by the operation of a $\text{Na}^+\text{-K}^+\text{-2Cl}^-$ cotransporter at the apical membrane, and the presence of $\text{Na}^+\text{-K}^+$ ATPase at the basolateral membrane. Cl^- conductance is necessary for the basolateral step of Cl^- absorption. CIC-K1 probably plays only a minor role, since Akzaki et al. [41] showed that there was no sodium loss in $\text{CIC-K1}^{-/-}$ mice. Accordingly, two additional Cl^- channels are thought to be expressed in the CTAL [24], which may compensate for the absence of CIC-K1.

ACKNOWLEDGMENTS

This work was supported by grants from the Agence Nationale de la Recherche (ANR) (ANR07-PHYSIO-008-2 and BLAN 2010-111201), and by a grant from the BHFZ (Bayerisch-Französisches Hochschulzentrum; FK-13/09). S. L'Hoste and O. Andrini hold ANR postdoctoral fellowships, and M. Keck, T. Grand and L. Pinelli PhD fellowships from the Ministère de l'Enseignement Supérieur et de la Recherche. The English text was edited by M. Ghosh.

REFERENCES

- [1] A. Vandewalle, F. Cluzeaud, M. Bens, S. Kieferle, K. Steinmeyer, T.J. Jentsch, Localization and induction by dehydration of ClC-K chloride channels in the rat kidney, *Am J Physiol* 272 (1997) F678-688.
- [2] R. Estevez, T. Boettger, V. Stein, R. Birkenhager, E. Otto, F. Hildebrandt, T.J. Jentsch, Barttin is a Cl⁻ channel beta-subunit crucial for renal Cl⁻ reabsorption and inner ear K⁺ secretion, *Nature* 414 (2001) 558-561.
- [3] K. Kobayashi, S. Uchida, S. Mizutani, S. Sasaki, F. Marumo, Intrarenal and cellular localization of CLC-K2 protein in the mouse kidney, *J Am Soc Nephrol* 12 (2001) 1327-1334.
- [4] C. Fahlke, M. Fischer, Physiology and pathophysiology of ClC-K/barttin channels, *Front Physiol* 1 (2010) 155.
- [5] D.B. Simon, R.S. Bindra, T.A. Mansfield, C. Nelson-Williams, E. Mendonca, R. Stone, S. Schurman, A. Nayir, H. Alpay, A. Bakaloglu, J. Rodriguez-Soriano, J.M. Morales, S.A. Sanjad, C.M. Taylor, D. Pilz, A. Brem, H. Trachtman, W. Griswold, G.A. Richard, E. John, R.P. Lifton, Mutations in the chloride channel gene, CLCNKB, cause Bartter's syndrome type III, *Nat Genet* 17 (1997) 171-178.
- [6] M. Konrad, M. Vollmer, H.H. Lemmink, L.P. van den Heuvel, N. Jeck, R. Vargas-Poussou, A. Lakings, R. Ruf, G. Deschenes, C. Antignac, L. Guay-Woodford, N.V. Knoers, H.W. Seyberth, D. Feldmann, F. Hildebrandt, Mutations in the chloride channel gene CLCNKB as a cause of classic Bartter syndrome, *J Am Soc Nephrol* 11 (2000) 1449-1459.
- [7] R. Birkenhager, E. Otto, M.J. Schurmann, M. Vollmer, E.M. Ruf, I. Maier-Lutz, F. Beekmann, A. Fekete, H. Omran, D. Feldmann, D.V. Milford, N. Jeck, M. Konrad, D. Landau, N.V. Knoers, C. Antignac, R. Sudbrak, A. Kispert, F. Hildebrandt, Mutation of BSND causes Bartter syndrome with sensorineural deafness and kidney failure, *Nat Genet* 29 (2001) 310-314.
- [8] K.P. Schlingmann, M. Konrad, N. Jeck, P. Waldegger, S.C. Reinalter, M. Holder, H.W. Seyberth, S. Waldegger, Salt wasting and deafness resulting from mutations in two chloride channels, *N Engl J Med* 350 (2004) 1314-1319.
- [9] Y. Matsumura, S. Uchida, Y. Kondo, H. Miyazaki, S.B. Ko, A. Hayama, T. Morimoto, W. Liu, M. Arisawa, S. Sasaki, F. Marumo, Overt nephrogenic diabetes insipidus in mice lacking the CLC-K1 chloride channel, *Nat Genet* 21 (1999) 95-98.
- [10] S. Adachi, S. Uchida, H. Ito, M. Hata, M. Hiroe, F. Marumo, S. Sasaki, Two isoforms of a chloride channel predominantly expressed in thick ascending limb of Henle's loop and collecting ducts of rat kidney, *J Biol Chem* 269 (1994) 17677-17683.
- [11] S. Kieferle, P. Fong, M. Bens, A. Vandewalle, T.J. Jentsch, Two highly homologous members of the ClC chloride channel family in both rat and human kidney, *Proc Natl Acad Sci U S A* 91 (1994) 6943-6947.
- [12] S. Waldegger, N. Jeck, P. Barth, M. Peters, H. Vitzthum, K. Wolf, A. Kurtz, M. Konrad, H.W. Seyberth, Barttin increases surface expression and changes current properties of ClC-K channels, *Pflugers Arch* 444 (2002) 411-418.
- [13] U. Scholl, S. Hebeisen, A.G. Janssen, G. Muller-Newen, A. Alekov, C. Fahlke, Barttin modulates trafficking and function of ClC-K channels, *Proc Natl Acad Sci U S A* 103 (2006) 11411-11416.
- [14] M. Fischer, A.G. Janssen, C. Fahlke, Barttin activates ClC-K channel function by modulating gating, *J Am Soc Nephrol* 21 (2010) 1281-1289.

- [15] C.J. Winters, W.B. Reeves, T.E. Andreoli, Cl⁻ channels in basolateral renal medullary membranes: III. Determinants of single-channel activity, *J Membr Biol* 118 (1990) 269-278.
- [16] C.J. Winters, W.B. Reeves, T.E. Andreoli, Cl⁻ channels in basolateral renal medullary membrane vesicles: IV. Analogous channel activation by Cl⁻ or cAMP-dependent protein kinase, *J Membr Biol* 122 (1991) 89-95.
- [17] C.J. Winters, W.B. Reeves, T.E. Andreoli, Cl⁻ channels in basolateral TAL membranes. XIV. Kinetic properties of a basolateral MTAL Cl⁻ channel, *Kidney Int* 55 (1999) 1444-1449.
- [18] R. Sauve, S. Cai, L. Garneau, H. Klein, L. Parent, pH and external Ca²⁺ regulation of a small conductance Cl⁻ channel in kidney distal tubule, *Biochim Biophys Acta* 1509 (2000) 73-85.
- [19] M. Paulais, J. Teulon, cAMP-activated chloride channel in the basolateral membrane of the thick ascending limb of the mouse kidney, *J Membr Biol* 113 (1990) 253-260.
- [20] R. Guinamard, A. Chraïbi, J. Teulon, A small-conductance Cl⁻ channel in the mouse thick ascending limb that is activated by ATP and protein kinase A, *J Physiol* 485 (1995) 97-112.
- [21] S. Lourdel, M. Paulais, P. Marvao, A. Nissant, J. Teulon, A chloride channel at the basolateral membrane of the distal-convoluted tubule: a candidate ClC-K channel, *J Gen Physiol* 121 (2003) 287-300.
- [22] A. Nissant, S. Lourdel, S. Baillet, M. Paulais, P. Marvao, J. Teulon, M. Imbert-Teboul, Heterogeneous distribution of chloride channels along the distal convoluted tubule probed by single-cell RT-PCR and patch clamp, *Am J Physiol Renal Physiol* 287 (2004) F1233-1243.
- [23] A. Nissant, M. Paulais, S. Lachheb, S. Lourdel, J. Teulon, Similar chloride channels in the connecting tubule and cortical collecting duct of the mouse kidney, *Am J Physiol Renal Physiol* 290 (2006) F1421-1429.
- [24] J. Teulon, S. Lourdel, A. Nissant, M. Paulais, R. Guinamard, P. Marvao, M. Imbert-Teboul, Exploration of the basolateral chloride channels in the renal tubule using the patch-clamp technique, *Nephron Physiol* 99 (2005) p64-68.
- [25] S. Waldegger, T.J. Jentsch, Functional and structural analysis of ClC-K chloride channels involved in renal disease, *J Biol Chem* 275 (2000) 24527-24533.
- [26] A. Diakov, K. Bera, M. Mokrushina, B. Krueger, C. Korbmacher, Cleavage in the {gamma}-subunit of the epithelial sodium channel (ENaC) plays an important role in the proteolytic activation of near-silent channels, *J Physiol* 586 (2008) 4587-4608.
- [27] B. Krueger, S. Haerteis, L. Yang, A. Hartner, R. Rauh, C. Korbmacher, A. Diakov, Cholesterol depletion of the plasma membrane prevents activation of the epithelial sodium channel (ENaC) by SGK1, *Cell Physiol Biochem* 24 (2009) 605-618.
- [28] N. Zerangue, B. Schwappach, Y.N. Jan, L.Y. Jan, A new ER trafficking signal regulates the subunit stoichiometry of plasma membrane K(ATP) channels, *Neuron* 22 (1999) 537-548.
- [29] S. Uchida, S. Sasaki, T. Furukawa, M. Hiraoka, T. Imai, Y. Hirata, F. Marumo, Molecular cloning of a chloride channel that is regulated by dehydration and expressed predominantly in kidney medulla, *J Biol Chem* 269 (1994) 19192.
- [30] S. Uchida, S. Sasaki, K. Nitta, K. Uchida, S. Horita, H. Nihei, F. Marumo, Localization and functional characterization of rat kidney-specific chloride channel, ClC-K1, *J Clin Invest* 95 (1995) 104-113.
- [31] A. Liantonio, M. Pusch, A. Picollo, P. Guida, A. De Luca, S. Pierno, G. Fracchiolla, F. Loiodice, P. Tortorella, D. Conte Camerino, Investigations of pharmacologic properties of the renal ClC-K1 chloride channel co-expressed with barttin by the use

of 2-(p-Chlorophenoxy)propionic acid derivatives and other structurally unrelated chloride channels blockers, *J Am Soc Nephrol* 15 (2004) 13-20.

- ~~S. Uchida, S. Sasaki, T. Furukawa, M. Hiraoka, T. Imai, Y. Hirata, F. Marumo, Molecular cloning of a chloride channel that is regulated by dehydration and expressed predominantly in kidney medulla, *J Biol Chem* 268 (1993) 3821-3824.~~
- [32] ~~A. Diakov, C. Korbmayer, A novel pathway of epithelial sodium channel activation involves a serum and glucocorticoid inducible kinase consensus motif in the C terminus of the channel's alpha-subunit, *J Biol Chem* 279 (2004) 38134-38142.~~
- [33] L. Feng, E.B. Campbell, Y. Hsiung, R. MacKinnon, Structure of a eukaryotic CLC transporter defines an intermediate state in the transport cycle, *Science* 330 (2010) 635-641.
- [33] C. Miller, Open-state substructure of single chloride channels from Torpedo electroplax, *Philos Trans R Soc Lond B Biol Sci* 299 (1982) 401-411.
- [34] ~~R. Dutzler, E.B. Campbell, M. Cadene, B.T. Chait, R. MacKinnon, X-ray structure of a ClC chloride channel at 3.0 Å reveals the molecular basis of anion selectivity, *Nature* 415 (2002) 287-294.~~
- [37] ~~R. Dutzler, E.B. Campbell, R. MacKinnon, Gating the selectivity filter in ClC chloride channels, *Science* 300 (2003) 108-112.~~
- [35] A.G. Janssen, U. Scholl, C. Domeyer, D. Nothmann, A. Leinenweber, C. Fahlke, Disease-causing dysfunctions of barttin in Bartter syndrome type IV, *J Am Soc Nephrol* 20 (2009) 145-153.
- [36] ~~G. Zifarelli, A. Liantonio, A. Gradogna, A. Picollo, G. Gramegna, M. De Bellis, A.R. Murgia, E. Babini, D.C. Camerino, M. Pusch, Identification of sites responsible for the potentiating effect of niflumic acid on ClC-Ka kidney chloride channels, *Br J Pharmacol* 160 (2010) 1652-1661.~~
- [37] A. Liantonio, A. Picollo, E. Babini, G. Carbonara, G. Fracchiolla, F. Liodice, V. Tortorella, M. Pusch, D.C. Camerino, Activation and inhibition of kidney CLC-K chloride channels by fenamates, *Mol Pharmacol* 69 (2006) 165-173.
- [38] T.Y. Chen, Structure and function of clc channels, *Annu Rev Physiol* 67 (2005) 809-839.
- [39] G. Rickheit, H. Maier, N. Strenzke, C.E. Andreescu, C.I. De Zeeuw, A. Muenscher, A.A. Zdebik, T.J. Jentsch, Endocochlear potential depends on Cl⁻ channels: mechanism underlying deafness in Bartter syndrome IV, *Embo J* 27 (2008) 2907-2917.
- [40] ~~S. Uchida, S. Sasaki, Function of chloride channels in the kidney, *Annu Rev Physiol* 67 (2005) 759-78.~~
- [41] ~~N. Akizuki, S. Uchida, S. Sasaki, F. Marumo, Impaired solute accumulation in inner medulla of Clcnk1^{-/-} mice kidney, *Am J Physiol Renal Physiol* 280 (2001) F79-87.~~

FIGURE LEGENDS

Fig. 1. Activation of mClC-K1 channels by mBarttin. *A*, steady-state current-voltage relationships obtained in ND96 solution for non-injected oocytes and oocytes expressing mBarttin or mClC-K1 alone, mClC-K1/mBarttin and mClC-K1/Y95A mBarttin. Each data point represents the mean from at least 30 oocytes from three different batches; SEM is shown by an error bar when this is larger than the symbols. *B*, representative original voltage-clamp recordings obtained from oocytes expressing mBarttin or mClC-K1 alone, mClC-K1/mBarttin, mClC-K1/Y95A mBarttin, and from non-injected oocytes.

Fig. 2. Increase in the surface expression of mClC-K1 channels produced by mBarttin. Currents at +60 mV correspond to the same data as in Fig. 1A. The cell surface expression values (measured in RLU, relative light units) were normalized relative to those found for mClC-K1/Y95A mBarttin in the same batch of oocytes. Each column represents the mean from at least 30 oocytes for current recordings, and from at least 30 oocytes from three different batches of oocytes for the surface expression. SEM is shown as an error bar when larger than the symbols. *, statistical difference ($P < 0.05$) between mBarttin, mClC-K1, mClC-K1/mBarttin or mClC-K1/Y95A mBarttin vs non-injected oocytes.

Fig. 3. Electrophysiological properties of mClC-K1/Y95A mBarttin channels at the whole-cell level in *X. laevis* oocytes. *A*, selectivity towards different anions. Steady-state current-voltage relationships were obtained when 80 mM extracellular Cl^- was replaced by Br^- ($n = 15$), NO_3^- ($n = 11$) or Γ ($n = 35$). SEM is shown as an error bar when larger than the symbols. *B*, effects of changes in extracellular Ca^{2+} concentration or pH on mClC-K1/Barttin or mClC-K1 activity. Currents at +60 mV were normalized to those of control (pH 7.4, 1.5

mM Ca^{2+}). Each column represents the mean from at least 6 oocytes from three different batches of oocytes; SEM is shown as an error bar when larger than the symbols (different extracellular pH values, $n = 6-11$; different Ca^{2+} concentrations, $n = 6-11$). *, statistical difference ($P < 0.05$) in comparison to pH 7.4, 1 mM Ca^{2+} .

Fig. 4. mClC-K1/mBarttin single-channel recordings channels in *X. laevis* oocytes. *A*, Representative current trace recorded at a holding potential (V_{hold}) of -70 mV from an outside-out patch. The binned current amplitude histogram (shown below the traces) was used to determine the single channel current amplitude. The dotted line labeled *C* in this figure and subsequent figures denotes the closed current level. The current level at which all channels are closed was determined by visual inspection (the trace with the least electrical noise). “Full” and “half” single-channel current levels are indicated by 1 and $\frac{1}{2}$, respectively. *B*, Representative current traces recorded at different holding potentials from an experiment similar to that described in *A*. *C*, Average current-voltage relationships ($n = 5-11$) calculated from recordings similar to those shown in *B*. Open and closed circles represent “full” and “half” single-channel openings, respectively. Vertical bars represent SEM values. Binned current amplitude histograms (not shown for clarity) were used to determine the single-channel current amplitude (i) at each holding potential. The dashed line represents a Goldman-Hodgkin-Katz fit (GHK-fit) of the data for a Cl^- selective channel. Single-channel conductance was calculated from the GHK-fit of the average current-voltage relationships using the “Patch for Windows” program (written by Dr. B. Letz; HEKA Electronics GmbH, Germany).

Fig. 5. mClC-K1/mBarttin channel anion selectivity determined at the single-channel level in *X. laevis* oocytes *A, B*. Representative single-channel current recordings obtained at a holding potential (V_{hold}) of +50 mV from an outside-out patch. Bars above the traces indicate the presence of NaCl, NaI, or NaBr in the bath solution. The insets show segments of the same current traces on an expanded time scale. The segments correspond to the time intervals indicated by the black bars below the traces. The single-channel current amplitudes for Cl^- and Br^- (i_{Cl^-} and i_{Br^-} , respectively) were determined as described in Fig. 4. No detectable single-channel current events were observed in the trace when NaI was present in the bath.

Fig. 6. Whole-cell recordings of mClC-K1/mBarttin in HEK293-transfected cells. *A*, representative, original, whole-cell recordings obtained from cells expressing mClC-K1/mBarttin channels. The pipette was filled with 150 mM Cl^- . Cells were bathed in a solution at pH 7.4 or pH 9.0, or in a solution where 140 mM extracellular Cl^- was replaced by Γ . *B*, steady-state current-voltage relationships obtained from cells expressing mClC-K1/mBarttin channels under the same conditions as described in panel A (pH 7.4, $n = 7$; pH 9.0, $n = 4$; Γ , $n = 4$). *C*, steady-state current-voltage relationships obtained from cells expressing mClC-K1/mBarttin channels. Pipette was filled with 33 mM Cl^- . Cells were bathed in physiological saline solution at pH 7.4 ($n = 7$) or pH 9.0 ($n = 7$), or in a solution where 140 mM extracellular Cl^- was replaced by Γ ($n = 7$).

Fig. 7. mClC-K1 single-channel activity in HEK293-transfected cells. *A*, representative mClC-K1 current recordings in the cell-attached configuration obtained at various voltages for cells expressing mClC-K1 channels in the presence or absence of mBarttin. Binned current amplitude histograms for -85 mV membrane potential are shown below the traces. Cells were bathed in physiological saline solution, with high- Cl^- solution in the pipette. *B*,

current-voltage relationships in the cell-attached configuration for cells expressing mClC-K1 channels with ($n = 3-11$) or without mBarttin ($n = 4$), and in the inside-out configuration for cells expressing mClC-K1 channels with mBarttin ($n = 4-7$). Pipettes were filled with a high-Cl⁻ solution. SEM is shown as an error bar when larger than the symbols. *C*, channel voltage dependence in the cell-attached and in the inside-out configurations. Channel activity (*NPo*) is plotted against membrane voltage (*V_m*). Each point is the mean of 4-7 values for the cell-attached configuration, and of 5-6 values for the inside-out configuration. Pipettes were filled with high-Cl⁻ solution. SEM is shown as an error bar.

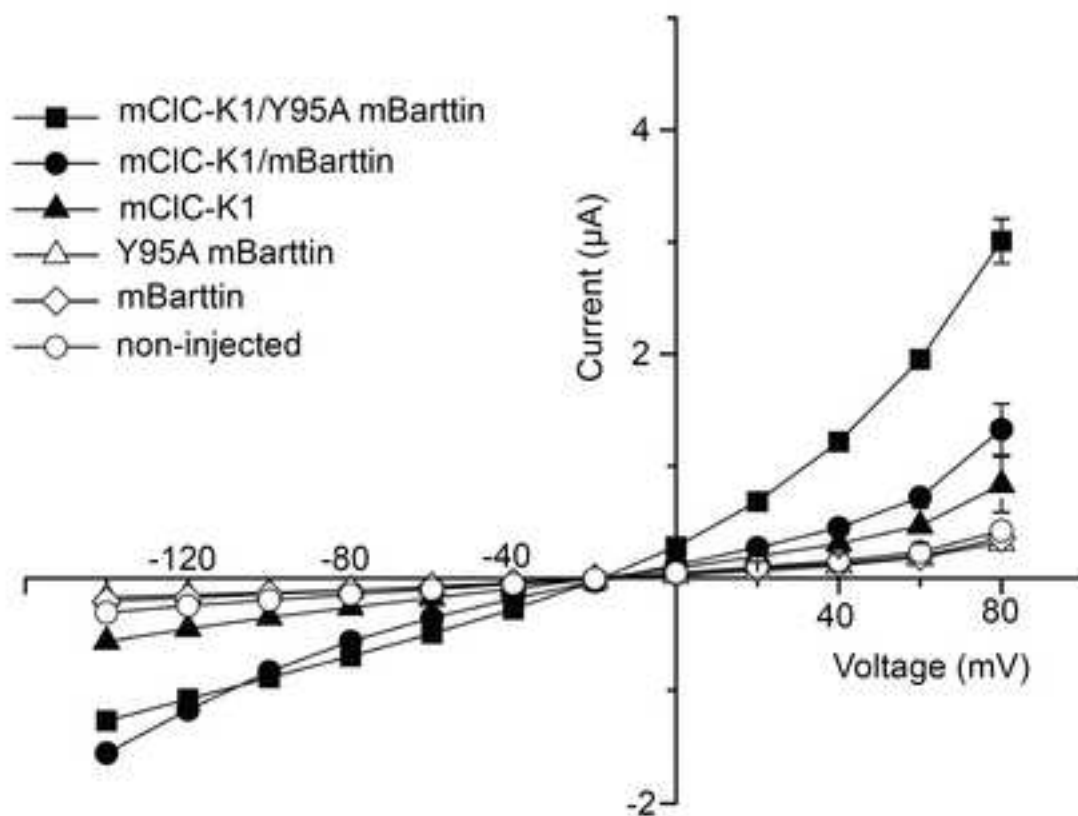
Fig. 8. Whole-cell recordings of V166E mClC-K1/mBarttin in HEK293-transfected cells. *A*, representative, original, whole-cell recordings. The pipette was filled with 150 mM Cl⁻. Cells were bathed in a solution at pH 7.4 or in a solution in which 140 mM extracellular Cl⁻ had been replaced by Γ. *B*, steady-state current-voltage relationships under the same conditions as described in panel A (pH 7.4, $n = 12$; Γ, $n = 14$).

Fig. 9. V166E mClC-K1 single-channel activity in cell-attached membrane patches from HEK293-transfected cells. *A*, representative V166E mClC-K1 current recordings obtained at various voltages for cells expressing mutant channels in the presence or in the absence of mBarttin. Binned current amplitude histograms for +85 mV membrane potential are shown below the traces. Cells were bathed in physiological saline solution, with a high-Cl⁻ solution in the pipette. *B*, current-voltage relationships for cells expressing mutant channels in the presence ($n = 3-4$) or in the absence ($n = 3-4$) of mBarttin. SEM is shown as an error bar when larger than symbols. *C*, channel voltage dependence. Channel activity (*NPo*) is plotted against membrane voltage (*V_m*). Each point is the mean of 3-4 values, with SEM shown as an error bar.

Fig. 9. Single-channel recordings from cell-attached membrane patches from intercalated cells of mouse OMCD. *A*, representative recordings obtained at various voltages. OMCD tubules were bathed in physiological saline solution, and the pipette contained a high-Cl⁻ solution containing 5 mM Ca²⁺. For clarity, the closed current level is not shown due to the large number of channels present in the membrane patch. *B*, current-voltage relationship ($n = 7$). Pipette contained high-Cl⁻ solution with 1 mM Ca²⁺. SEM is shown as error bars when larger than symbols. *C*, effects of changing the Ca²⁺ concentration in the pipette on the number of channels (1 mM Ca²⁺, $n = 5$; 5 mM Ca²⁺, $n = 3$). *, statistical difference ($P < 0.05$) in comparison to 1 mM Ca²⁺.

Figure 1
[Click here to download high resolution image](#)

A



B

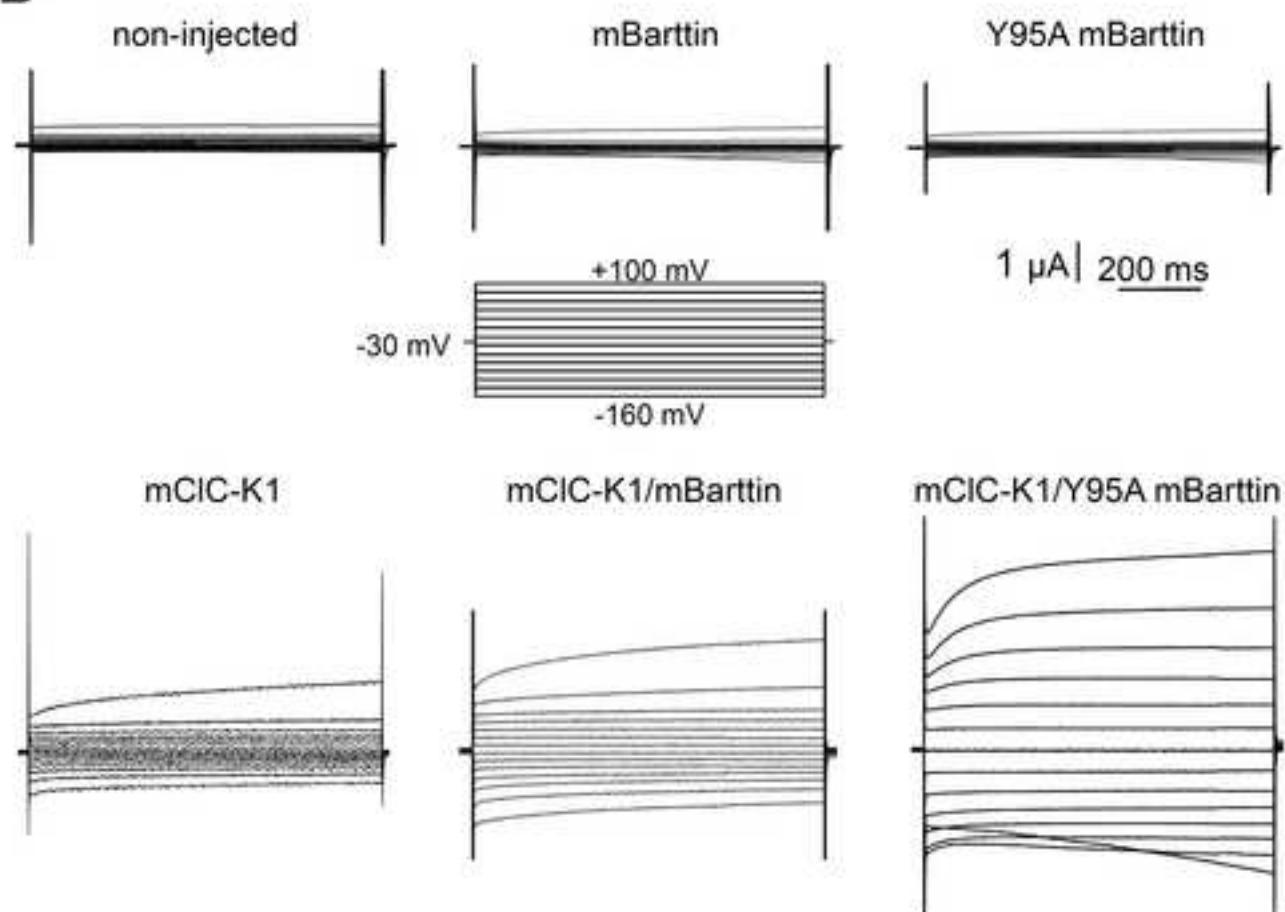


Figure 1

Figure 2
[Click here to download high resolution image](#)

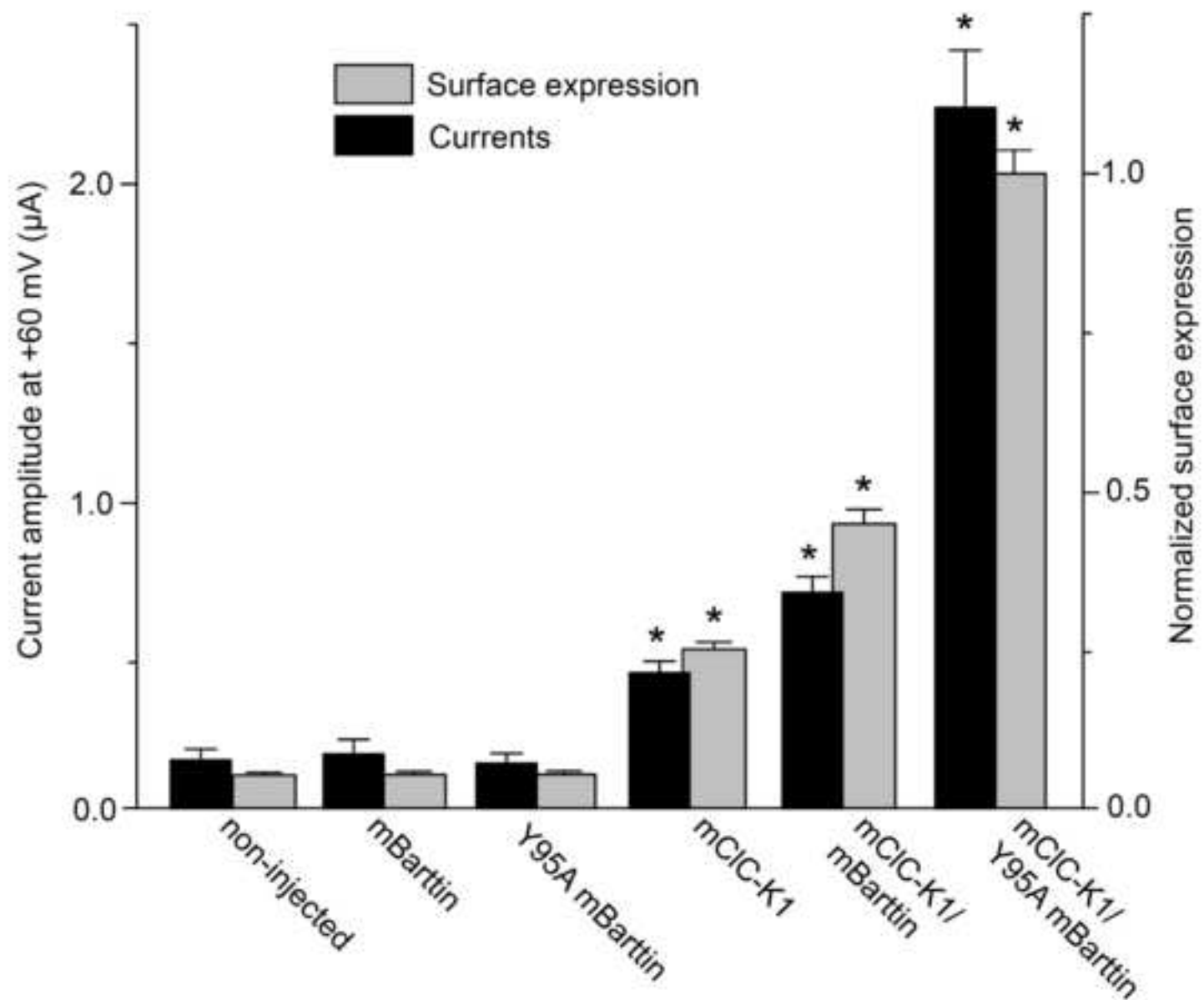


Figure 2

Figure 3
[Click here to download high resolution image](#)

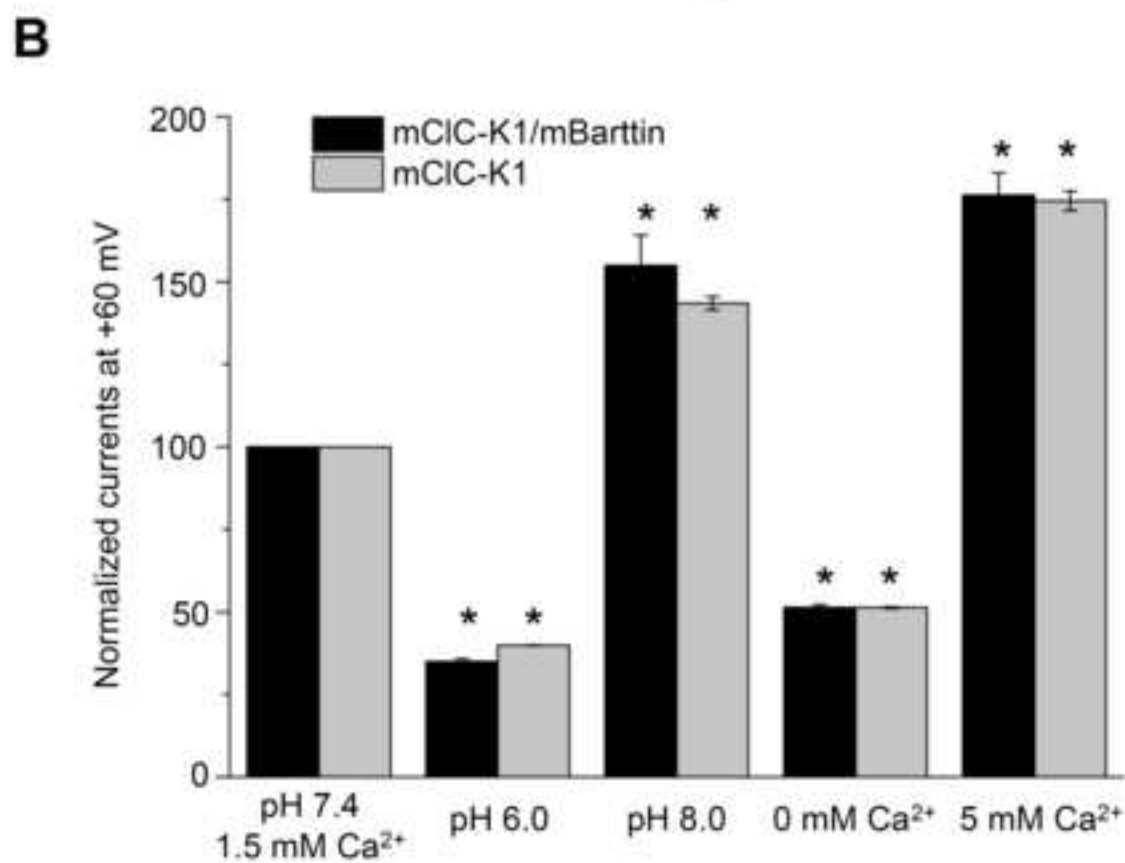
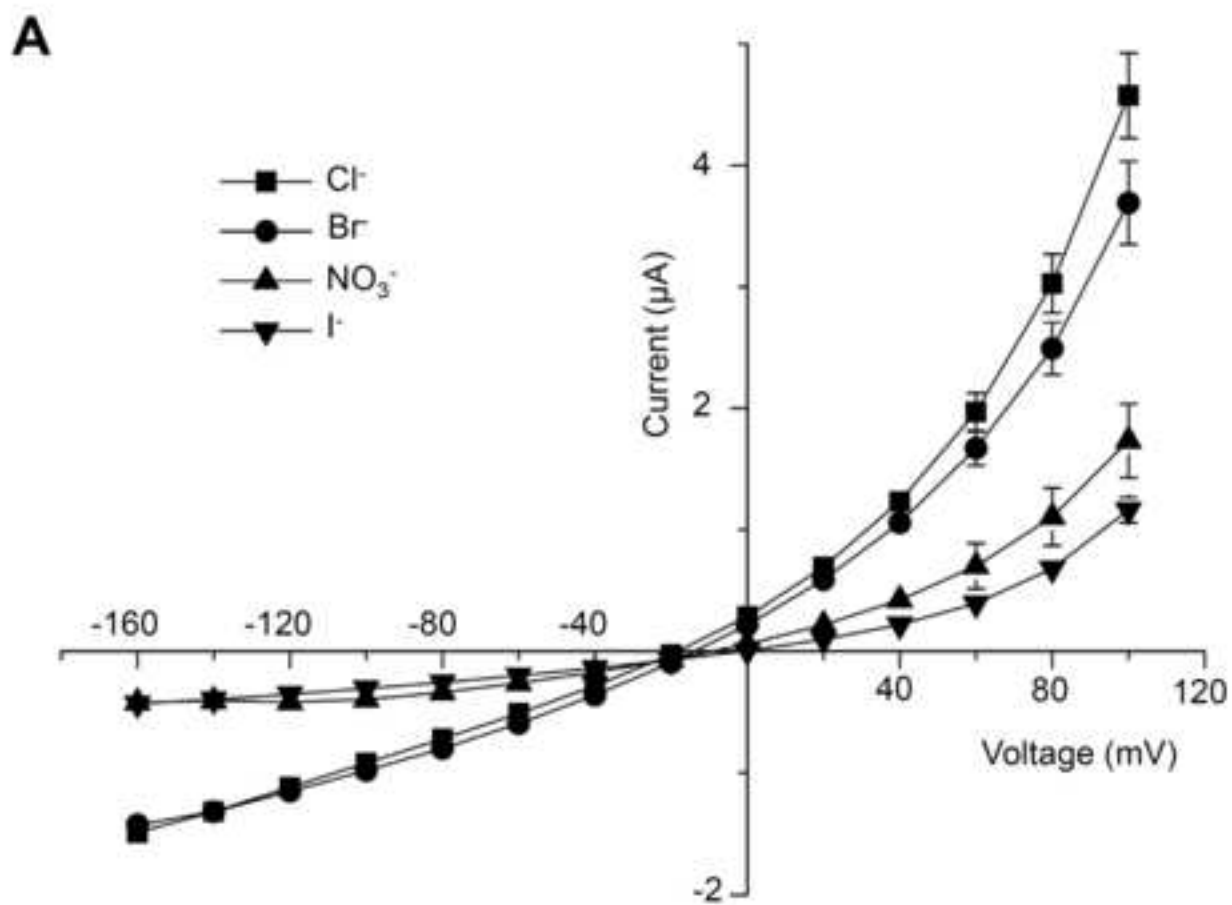


Figure 3

Figure 4
[Click here to download high resolution image](#)

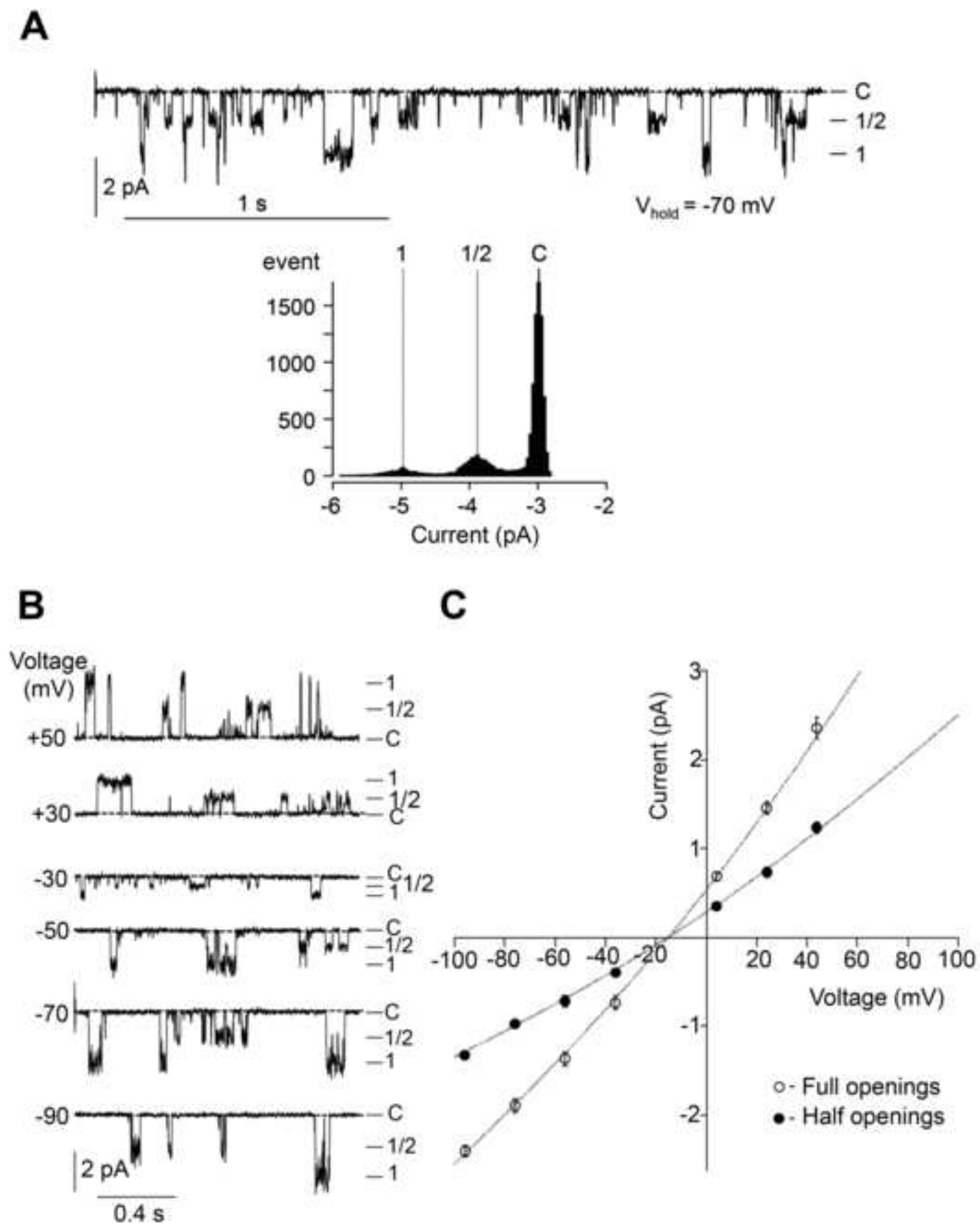


Figure 4

Figure 5
[Click here to download high resolution image](#)

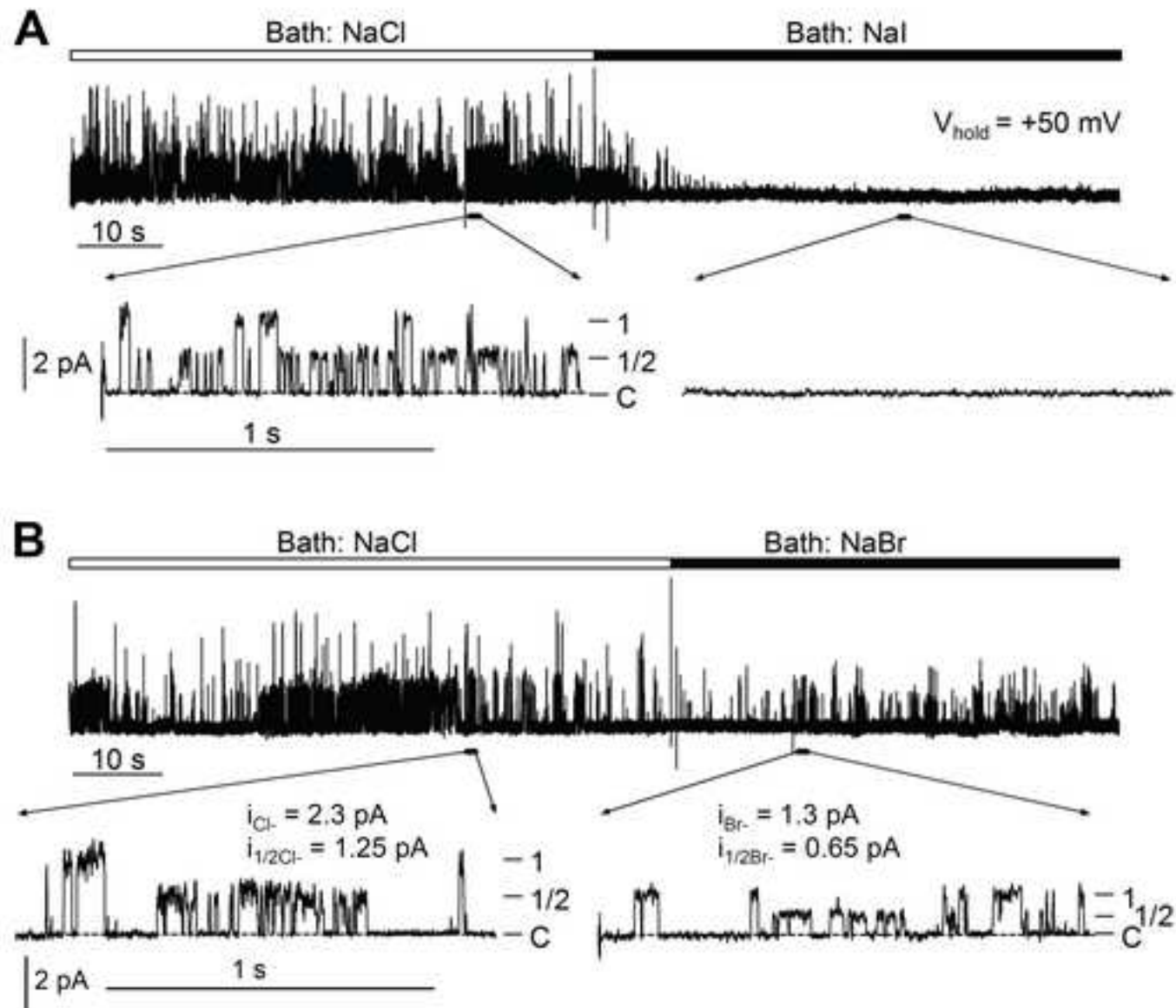


Figure 5

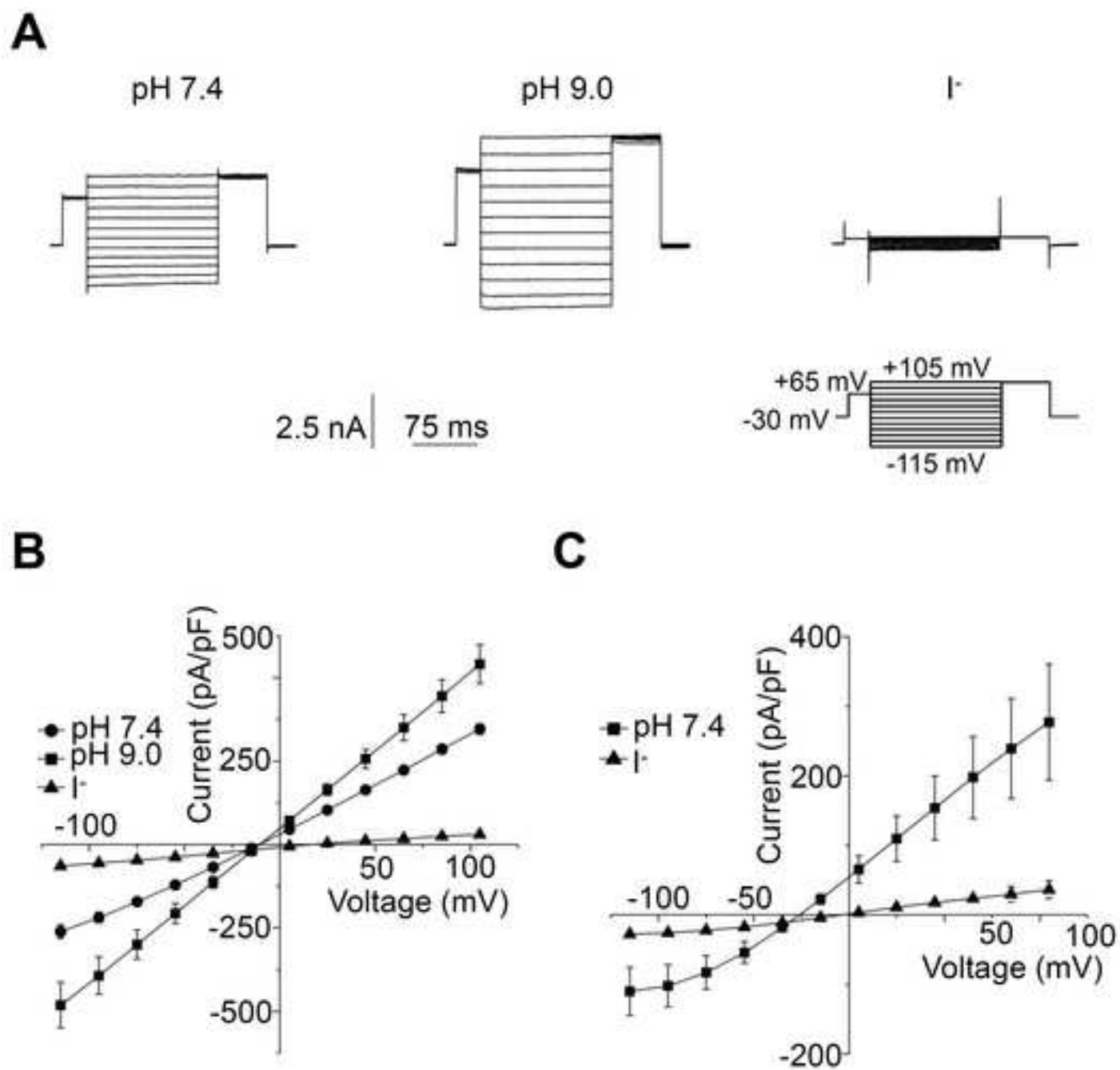


Figure 6

Figure 7
[Click here to download high resolution image](#)

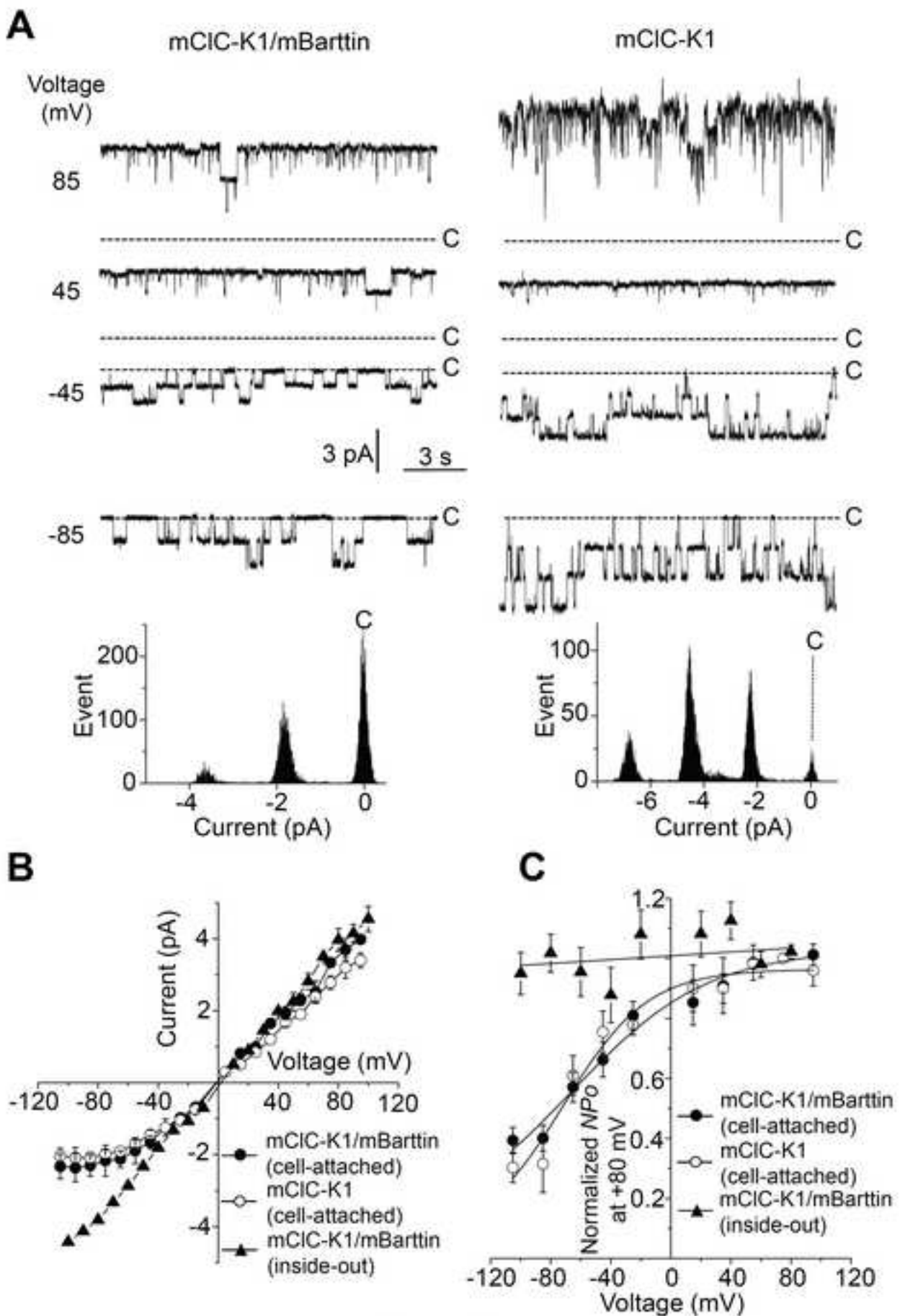


Figure 7

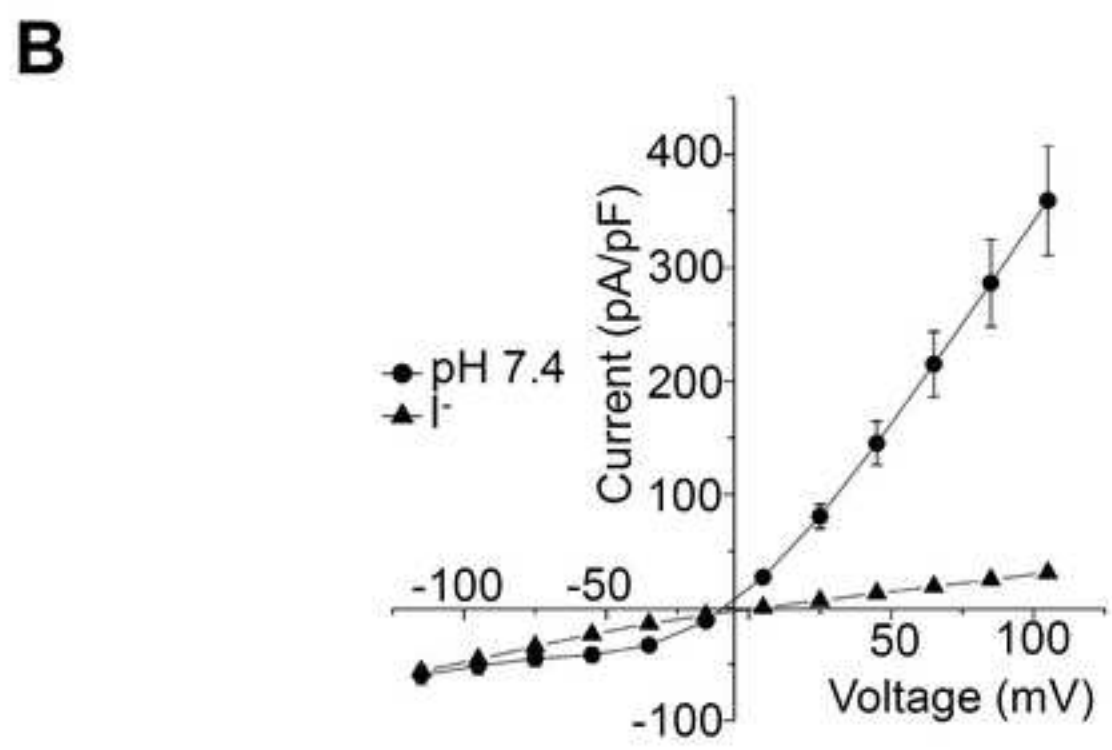
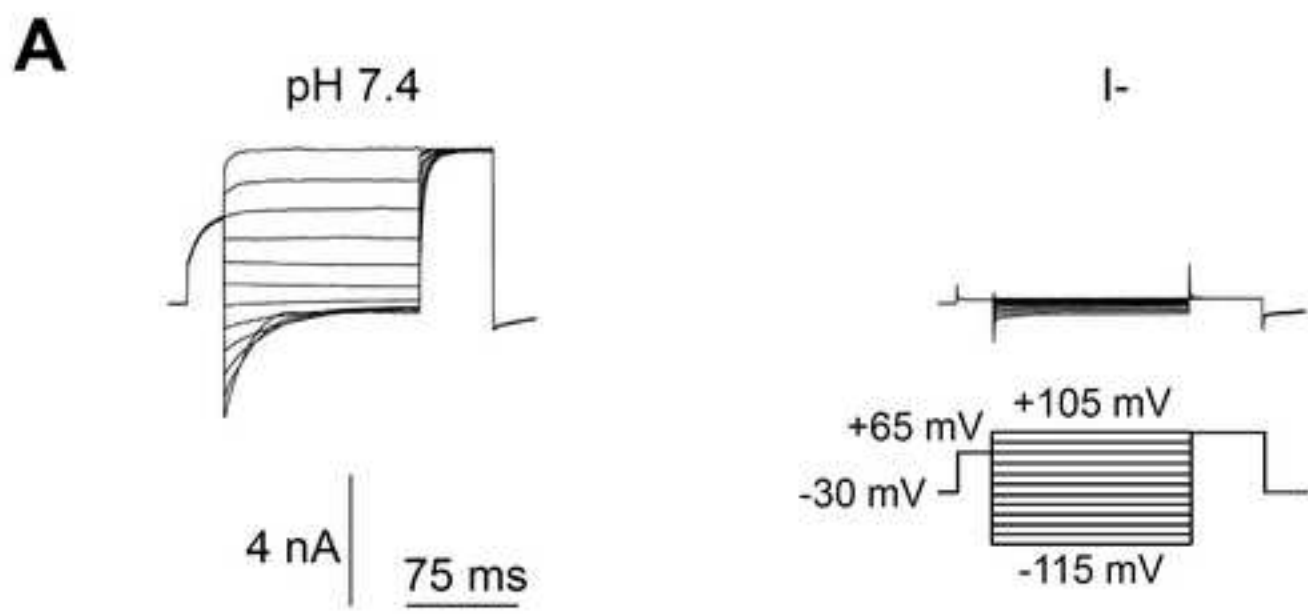


Figure 8

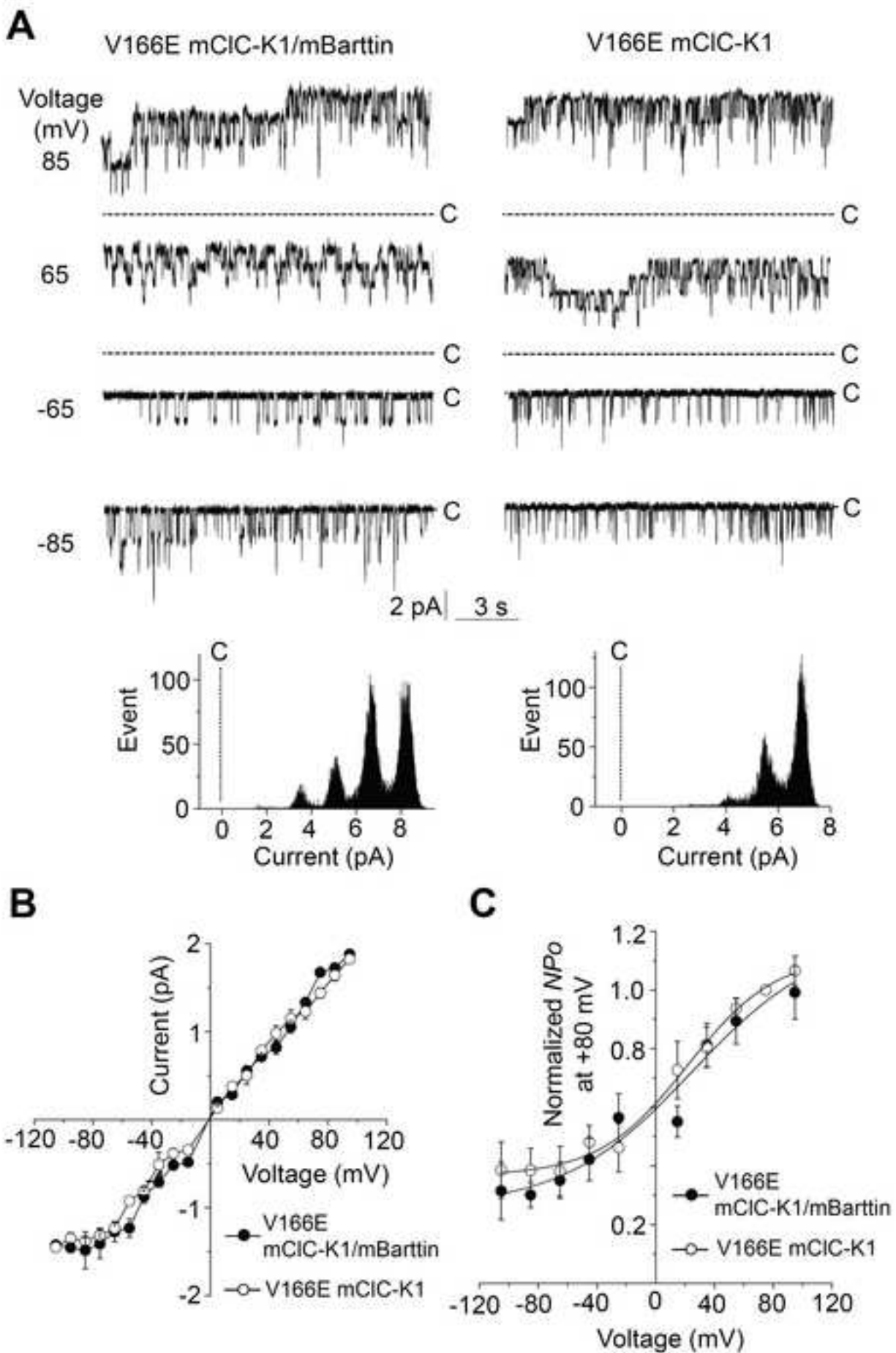


Figure 9